DR-318

Fe-2028-13
Dist. Category UC-90d

KINETICS AND MECHANISM OF DESULFURIZATION AND DENITROGENATION OF COAL-DERIVED LIQUIDS

Eleventh Quarterly Report for Period

December 21, 1977, to March 20, 1978

Prepared by:

Bruce C. Gates, James R. Katzer
Jon H. Olson, Harold Kwart, and Alvin B. Stiles

Departments of Chemical Engineering and Chemistry
University of Delaware
Newark, Delaware 19711

Date Published

May 20, 1978

Prepared for

Fossil Energy
Energy Research and Development Administration
Washington, D.C.

Under Contract No. E(49-18)-2028

DISCLAIMER

Available from:

National Technical Information Service (NTIS)
U.S. Department of Commerce
5285 Port Royal Road
Springfield, Virginia 22161

Price: Printed copy: $5.25
Microfiche: $3.00

TABLE OF CONTENTS

LIST OF TABLES

List of Figures

List of Figures (Continued)

1. ABSTRACT

Three high-pressure flow microreactors and two batch autoclave reactors have been used to study the reaction networks and kinetics of (1) catalytic hydrodesulfurization of dibenzothiophene and methyl-substituted dibenzothiophenes and (2) catalytic hydrodenitrogenation of quinoline, methyl-substituted quinolines, acridine, benzacridines, dibenzacridine, and carbazole. The catalysts were commercial, sulfided $CoO-MoO_3/\gamma-Al_2O_3$, $NiO-MoO_3/\gamma-Al_2O_3$, and $NiO-WO_3/\gamma-Al_2O_3$.

At the typical conditions of 300°C and 104 atm, dibenzothiophene reacts to give H_2S and biphenyl in high yield, but there is some hydrogenation preceding desulfurization. Methyl-substituted dibenzothiophenes react similarly, and each reaction is first-order in the sulfur-containing compound. Two methyl groups near the sulfur atom (in the 4 and 6 positions) reduce the reactivity tenfold, whereas methyl groups in positions further removed from the sulfur atom increase reactivity about twofold. The results are consistent with steric and inductive effects influencing adsorption. The data indicate competitive adsorption among the sulfur-containing compounds.

Hydrodesulfurization of multiring sulfur-containing compounds show that the reactivity decreases with increasing number of rings in the compound; but the same does not apply to the four-ring compound (i.e., benzonaphthothiophene) which has higher reactivity than that of the 3-ring compound (i.e., dibenzothiophene).

In quinoline hydrodenitrogenation, both rings are typically saturated before the C-N bond is broken. Similarly, in acridine conversion a large amount of hydrogenation precedes nitrogen removal. Breaking of the carbon-nitrogen bond is evidently one of the slower reactions in the network. The Ni-Mo catalyst is about twice as active as the Co-Mo catalyst for ring hydrogenation, and the two catalysts are about equally active for breaking the carbon-nitrogen bond.

Reactivity of carbazole is slightly lower than that of quinoline but higher than that of acridine. Again, extensive hydrogenation precedes heteroatom removal. The relative activity of nitrogen-containing compounds at 367°C and 136 atm decreases according to: quinoline (2.52), carbazole (2.43), acridine (1.62) and benz[c]acridine (1.54) where the numbers in parentheses are pseudo first-order rate constants in min^{-1}.

Preliminary studies of competing hydroprocessing reactions involving quinoline, indole and naphthlene over $Ni-Mo/\gamma-Al_2O_3$ have shown that the naphthalene hydrogenation rate is markedly reduced by the presence of quinoline; whereas the reactivity of quinoline is virtually unaltered by the presence of naphthalene. Similarly the rate of hydrodenitrogenation of indole is strongly reduced by the presence of quinoline, whereas the rate of hydrodenitrogenation of quinoline is unaffected by the presence of indole.

Aged catalysts taken from the H-Coal® and Synthoil processes contained coke and deposits of mineral matter (primarily FeS, titanium and clays). The H-Coal catalysts were examined, for example, in experiments with dibenzothiophene hydrodesulfurization and quinoline hydrodenitrogenation. The activity of the used catalyst was reduced 20-fold for hydrodesulfurization of dibenzothiophene and fivefold for hydrodenitrogenation of quinoline. Most of the loss of hydrodesulfurization activity was associated with the mineral deposits and not with the coke.

II. OBJECTIVES AND SCOPE

The major objectives of this research are as follows:

i) to develop high-pressure liquid-phase microreactors for operation in pulse and steady-state modes to allow determination of quantitative reaction kinetics and catalytic activities in experiments with small quantities of reactants and catalyst.

ii) To determine reaction networks, reaction kinetics, and relative reactivities for catalytic hydrodesulfurization of multi-ring aromatic sulfur-containing compounds found in coal-derived liquids.

iii) To determine reaction networks, reaction kinetics, and relative reactivities for catalytic hydrodenitrogenation of multi-ring aromatic nitrogen-containing compounds found in coal-derived liquids.

iv) To obtain quantitative data characterizing the chemical and physical properties of aged hydroprocessing catalysts used in coal liquefaction processes and to establish the mechanisms of deactivation of these hydroprocessing catalysts.

v) To develop reaction engineering models for predicting the behavior of coal-to-oil processing and of catalytic hydroprocessing of coal-derived liquids and to suggest methods for improved operation of hydrodesulfurization and hydrodenitrogenation processes.

vi) In summary, to recommend improvements in processes for the catalytic hydroprocessing of coal-derived liquids.

SCOPE

A unique high-pressure, liquid-phase microreactor is being developed for pulse (transient) and steady-state modes of operation for kinetic measurements to achieve objectives ii) through iv). The relative reactivities of the important types of multi-ring aromatic compounds containing sulfur and nitrogen are being measured under industrially important conditions (300-450°C and 500-4000 psi). The reaction networks and kinetics of several of the least-reactive multi-ring aromatic sulfur-containing and nitrogen-containing compounds commonly present in coal-derived liquids will be determined. Catalyst deactivation is an important aspect of the commercial scale upgrading of coal-derived liquids. Accordingly, the chemical and physical properties of commercially aged coal-processing catalysts are being determined to provide an understanding of catalyst deactivation; these efforts can lead to improved catalysts or procedures to minimize the problem. To make the results of this and related research most useful to ERDA, reaction engineering models of coal-to-coal processing in trickle-bed and slurry-bed catalytic reactors including deactivation will be developed to predict conditions for optimum operation of these processes. Based on the integrated result of all of the above work, recommendations will be made to ERDA for improved catalytic hydrodesulfurization and hydrodenitrogenation processing.

III. SUMMARY OF PROGRESS TO DATE

This summary is organized to parallel the task statements of the contract. A milestone chart is provided at the end of this section.

Microreactor Development

Three continuous-flow, liquid-phase, high-pressure microreactors have been built and operated under this contract. The work in this report confirms the success of these microreactors; the data from the batch autoclave runs are effectively identical to data from the flow microreactors. This task has been completed.

Catalytic Hydrodesulfurization

The hydrodesulfurization of dibenzothiophene (DBT) has been examined with a high-pressure microreactor and in batch, stirred-autoclave experiments. The range of data show that the reaction network is slightly more complex than the direct reduction of dibenzothiophene (DBT) to hydrocarbon products; the network is the following at 300°C and 100 atm:

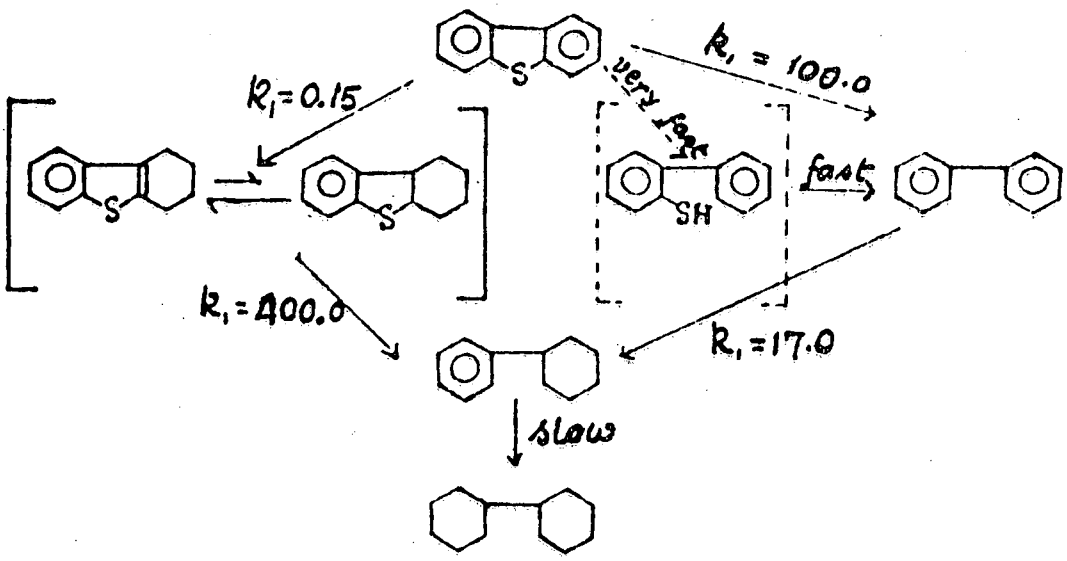

The relative rates of hydrodesulfurization of a variety of the important sulfur-containing compounds in coal-derived liquids have been determined. The compounds include methyl-substituted dibenzothiophenes, which evidently are among the least reactive compounds in hydrodesulfurization. The relative rate constants for the various reactants are the following: BT, very large; DBT, 1; 4-MeDBT, 0.16; 4,6-diMeDBT, 0.10; 3,7-diMeDBT, 1.7; and 2,8-diMeDBT, 2.6. These results are largely explained by steric and inductive effects. Groups located near the 'S' atom restrict its interaction with a surface anion vacancy and lower the reactivity. Inductive effects explain the higher reactivities of the compounds having methyl substituents where they exert no steric influence.

The reactivities of the compounds have been determined with individual sulfur-containing compounds and with pairs of these compounds. The reactivities of these compounds are influenced by competitive adsorption determined by the previously mentioned steric and inductive effects.

More detailed study of the hydrodesulfurization of 4,6-dimethyldibenzothiophene, which is the least reactive sulfur-containing compound found so far, shows that the reaction network is similar to that of dibenzothiophene but that hydrogenation of the aromatic ring is more pronounced than for dibenzothiophene.

Results from batch-autoclave reactor studies on the hydrodesulfurization of multi-ring sulfur-compounds (with sulfided Co-Mo/γ-Al_2O_3, 300°C and 70 $\pm$ 2 atm of H_2) show that the reactivity decreases from 1-ring to 3-ring compounds and then it increases for the 4-ring compound. Thus the three-ring sulfur-compound, dibenzothiophene and its methyl derivatives are the least reactive compounds studied so far. The first-order rate constants for the hydrodesulfurization of these compounds are given below:

Reactant	Pseudo first-order rate Constant, cm^3/g cat h
thiophene	5000
benzothiophene	2900
dibenzothiophene	200
benzonaphthothiophene	600
7,8,9,10-tetrahydrobenzo-naphthothiophene	280

Three different catalysts, namely Co-Mo/γ-Al_2O_3, Ni-Mo/γ-Al_2O_3 and Ni-W/Al_2O_3 have been tested for the hydrodesulfurization of dibenzothiophene. The activities of these catalysts have been found to decrease in the order: Ni-Mo > Ni-W $\geq$ Co-Mo.

Catalytic Hydrodenitrogenation

The hydrodenitrogenation of quinoline has been studied to yield a nearly complete identification of the reaction network and partial identification of the rate parameters in this network. The network is as follows:

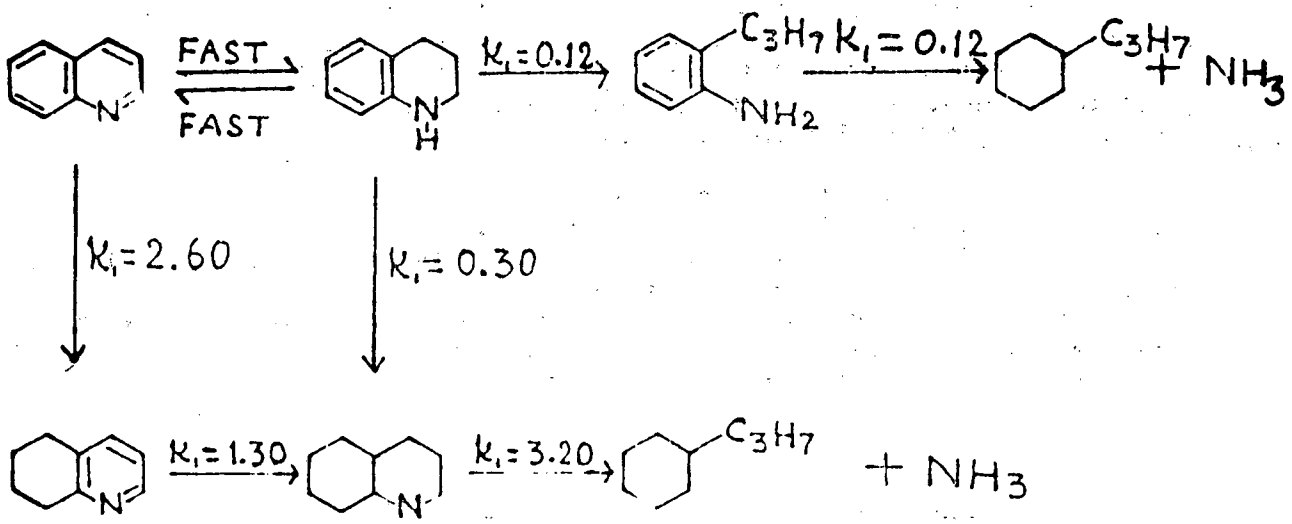

This network shows that usually both the benzene and pyridine rings are saturated before the C-N bond in the (now) piperidine ring is broken. Thus, the hydrodenitrogenation of quinoline requires a large consumption of hydrogen before the nitrogen atom is removed from the hydrocarbon structure. The lack of selectivity encountered in hydrodenitrogenation stands in sharp contrast to the high selectivity in hydrodesulfurization.

The total rate of hydrodenitrogenation shows a maximum with respect to hydrogen partial pressure. This is because the pseudo first-order rate constant for the C-N bond scission step is reduced by increasing hydrogen pressure and the rate constants for the hydrogenation steps, which increase with hydrogen pressure at lower hydrogen pressures, pass through a maximum and decrease with increasing hydrogen pressure at the high hydrogen pressures.

Also in hydrodenitrogenation of acridine, a large amount of hydrogenation precedes nitrogen removal, and the carbon-nitrogen bond breaking reactions are relatively slow. In the presence of Co-Mo/γ-Al_2O_3 catalyst, heteroaromatic ring hydrogenation is favored, and with a Ni-Mo/γ-Al_2O_3 catalyst, aromatic ring hydrogenation is favored. For both acridine and quinoline, little effect of replacing Co with Ni could be detected in the nitrogen removal reaction, although Ni-Mo/γ-Al_2O_3 is roughly twice as active for hydrogenation as Co-Mo/γ-Al_2O_3.

The hydrodenitrogenation of carbazole has been examined under conditions similar to those used for acridine. Both carbazole disappearance and total nitrogen removal can be represented as first-order reactions. Tetrahydrocarbazole was the major intermediate compound present in the dry column extract. Both cis-hexahydrocarbazole and octahydrocarbazole were identified as minor products. Reactivity of carbazole is slightly less than that of quinoline and acridine is the least reactive. Hydrodenitrogenation of four- and five-ring nitrogen-containing compounds are currently being studied.

Preliminary experiments have been carried out to characterize hydrodenitrogenation of substituted quinolines. The conditions used were similar to those used for quinoline hydrodenitrogenation. 2,6-, 2,7- and 2,8-dimethylquinolines were studied and products identified were analogous to those observed in the quinoline network. The reactivity of these compounds to hydrodenitrogenation is comparable to that of quinoline.

The reaction network for the hydrodenitrogenation of acridine (in White Oil) catalyzed by Ni-Mo/γ-Al_2O_3 catalyst is as given below:

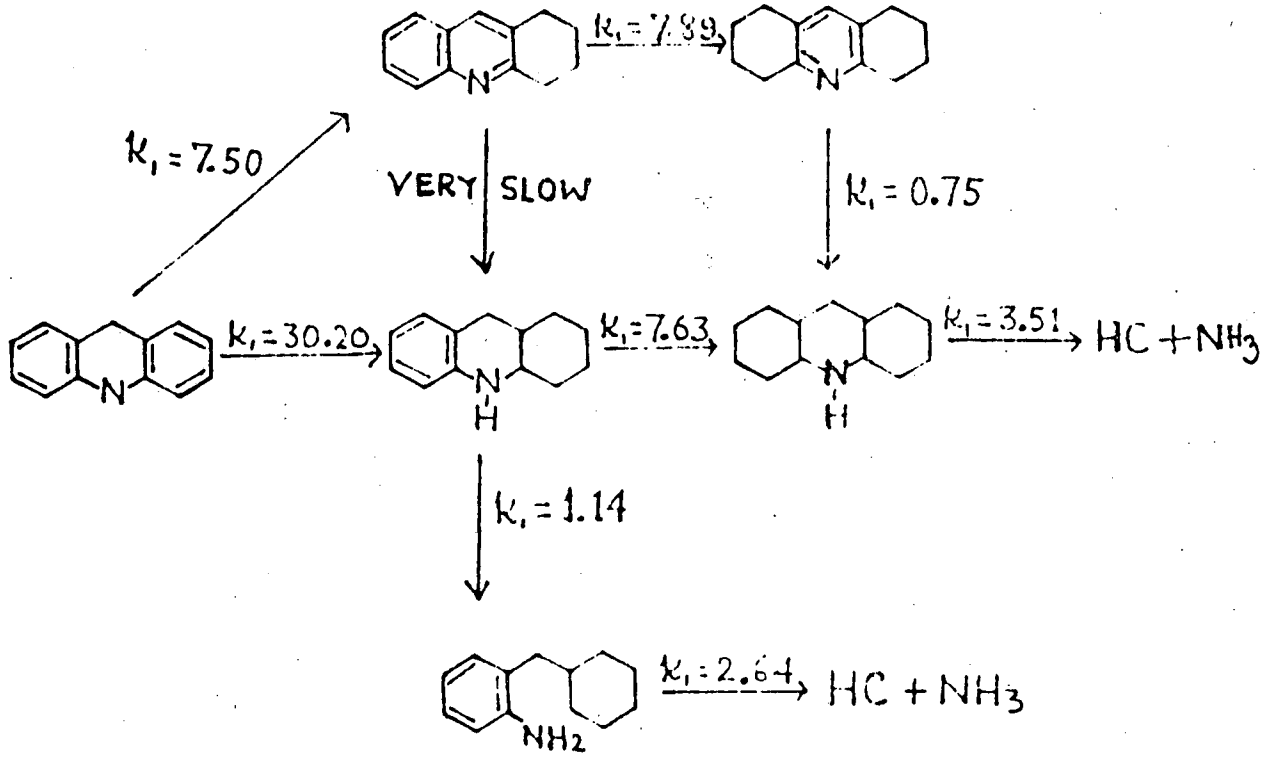

The pseudo first-order rate constants are for 367°C and 136 atm. The pseudo first-order rate constants for hydrodenitrogenation (total nitrogen removal) at 367°C and 136 atm catalyzed by Ni-Mo/ -Al_2O_3 falls in the following order:

Reactant	Pseudo first-order rate constant for total nitrogen removal, min^{-1}
Dibenz[c,h]acridine	3.79
Quinoline	2.52
Carbazole	2.43
Acridine	1.62
Benz[c]acridine	1.54
Benz[a]acridine	1.08

Preliminary studies of competing hydroprocessing reactions catalyzed by Ni-Mo/γ-Al_2O_3 and involving quinoline, indole and naphthalene in White Oil show that marked interactions exist. The naphthalene hydrogenation rate is markedly reduced by the presence of quinoline; whereas the reactivity of quinoline is virtually unchanged by the presence of naphthalene. Similarly the rate of hydrodenitrogenation of indole, a non-basic nitrogen-containing compound, is strongly reduced by the presence of quinoline, whereas the rate of hydrodenitrogenation of quinoline, a basic nitrogen-containing compound, is unaffected by the presence of indole. Studies involving combinations of nitrogen- and sulfur-containing compounds and aromatic hydrocarbons are underway.

Catalyst Deactivation

A variety of physical techniques have been used to identify the aging process for catalysts used in synthetic liquid fuel processes. Catalyst samples from three processes have been examined: a proprietary fixed-bed process, Synthoil, and H-Coal^R. The spent fixed-bed catalysts show the formation of an external crust which appears to be formed by columnar grain growth combined with the deposition of coal mineral matter, particularly clays and rutile. This external crust is absent from the H-Coal^R catalyst. The interior of the catalyst is altered by several processes: coking, reactive deposition of mineral matter, passive deposition of mineral matter, and crack enhancement. These four processes are found in catalysts from all three processes. Coking fills the micropore volume of the catalyst. Reactive deposition of mineral matter penetrates about 200 μm from the outer surface into the interior of the catalyst. The concentration profile is approximately exponentially decreasing from the exterior surface. Passive cementing occurs within 50 μm of the surface unless the irregular concentration profiles. Finally, grain growth can occur inside the catalyst near the surface and tends to increase these cracks. When the surface cracks become a significant portion of the pore volume, passive deposition can penetrate further into the interior of the catalyst.

The activity of aged catalyst from the H-Coal^R process has been measured in batch experiments with dibenzothiophene and with quinoline. The activity was reduced 20-fold for hydrodesulfurization of dibenzothiophene and five-fold for hydrodenitrogenation of quinoline. Burning off of carbonaceous deposits increased the activity of the aged catalyst only

three-fold for dibenzothiophene hydrodesulfurization, which implies that irreversibly deposited inorganic matter was responsible for most of the loss of catalytic activity.

Microreactor Engineering

The use of moments as a tool in interpreting pulse data from microreactors has been extended to fairly complex reaction networks. This work is now complete. The complex data from quinoline and acridine reactions have been reduced to rate parameters by extension of nonlinear regression analysis. Reaction engineering concerned with coal hydroprocessing is now underway.

TIME PLAN* AND MILESTONE CHART**

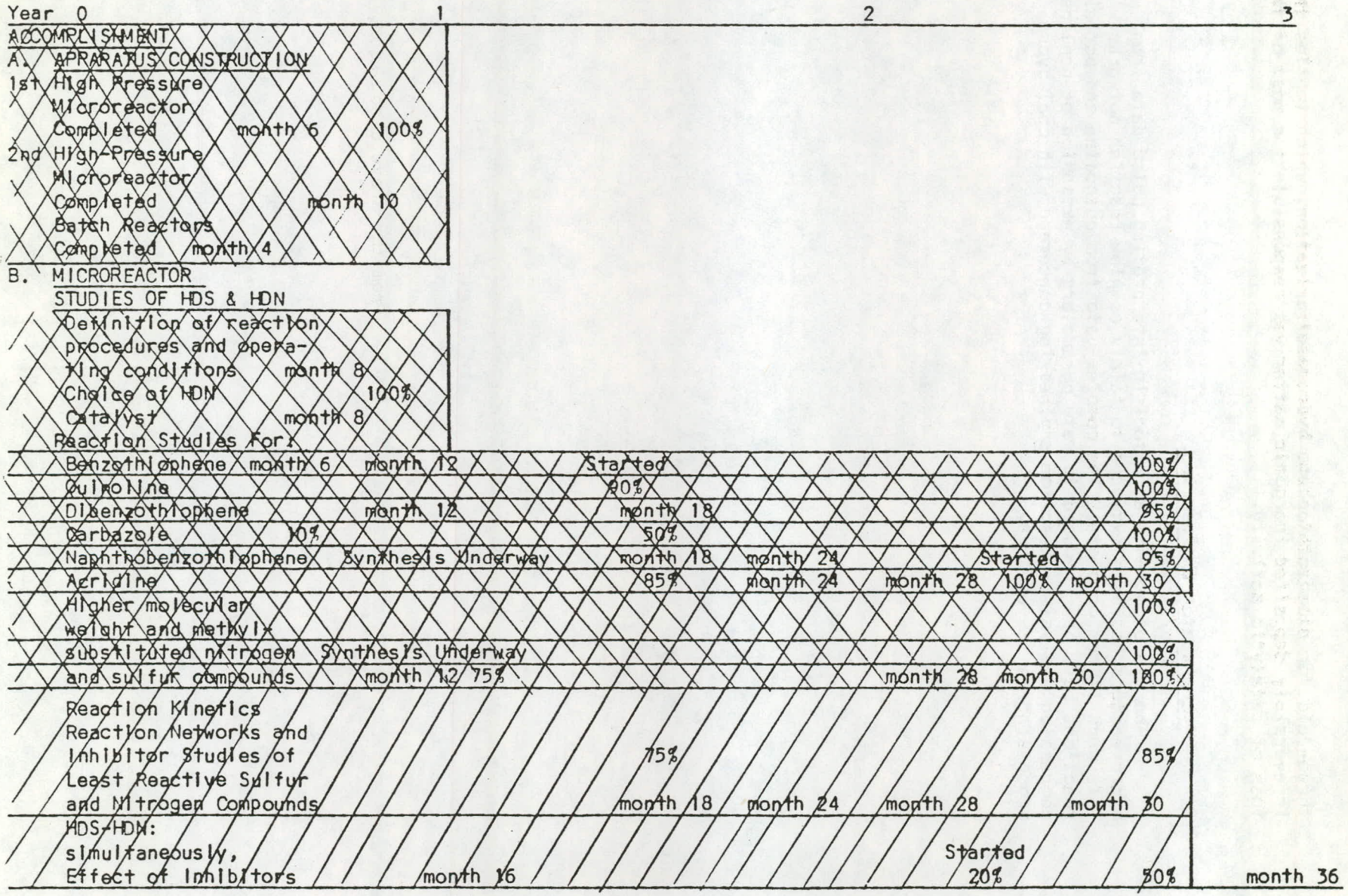

TIME PLAN* AND MILESTONE CHART** (Cont)

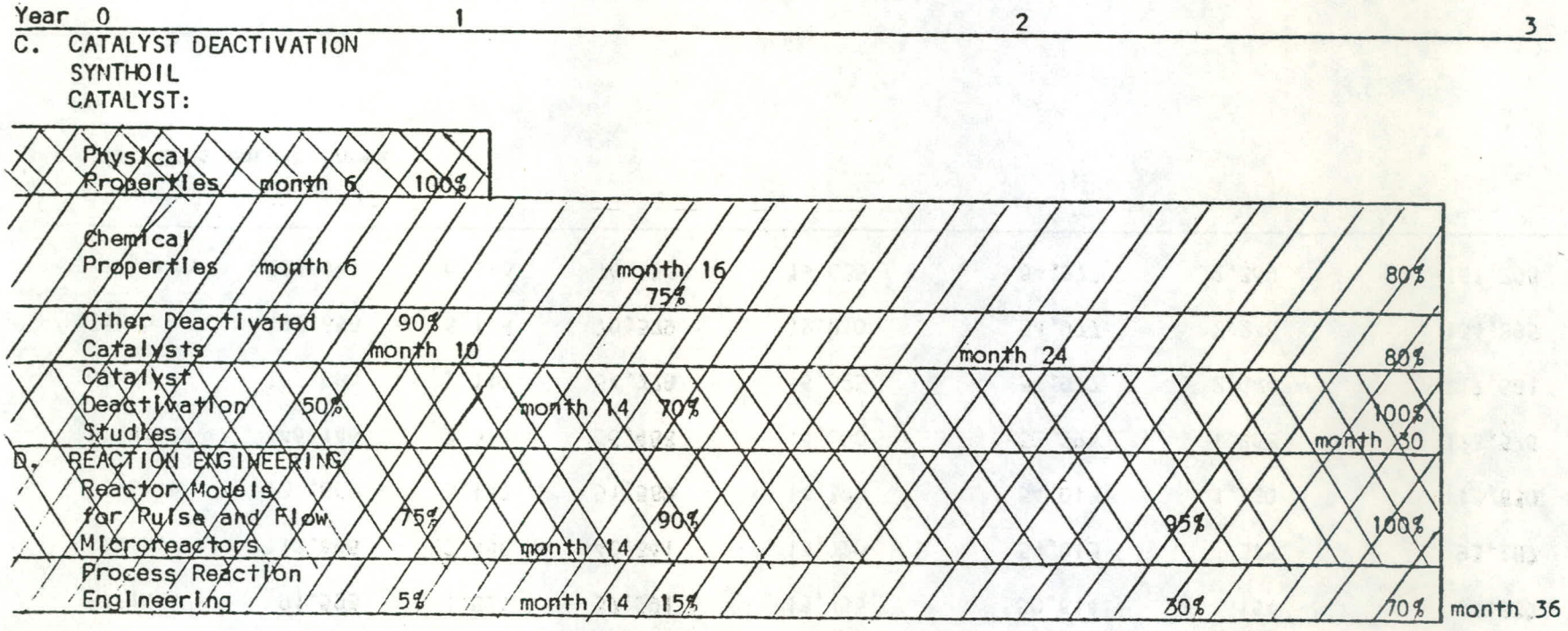

*Time Plan and Milestone Chart as Presented in Proposal.

**Hatching indicates that activity indicated is under active investigation; number in hatch region indicates the percentage completed; crosshatching indicates that the task has been completed.

CUMULATIVE EXPENDITURES*

Quarter	Personnel	Travel	Supplies & Expenses	Occupancy & Maintenance	Equipment	Information Processing	Transfers (Overhead)
First	$ 5,807	$ 28	$ 4,674	$ 6,110	$ 610	--	--
Second	20,740	528	10,007	9,208	17,978	--	$ 10,202
Third	37,396	1,152	19,582	10,108	30,704	--	20,035
Fourth	53,418	1,152	25,735	10,634	34,930	$ 97	38,710
Fifth	91,593	1,521	37,291	13,755	50,614	154	75,839
Sixth	112,666	2,458	42,341	13,920	54,013	375	93,287
Seventh	132,669	3,140	51,589	14,396	54,013	1,180	113,830
Eighth	146,146	3,814	56,488	14,600	52,295	1,868	123,576
Ninth	167,884	5,119	54,778	16,325	54,977	2,044	117,681
Tenth	192,658	6,113	70,579	18,010	54,977	2,248	134,895
Eleventh	224,941	6,113	76,733	19,635	54,977	2,369	161,208

*Includes encumbrances

IV. DETAILED DESCRIPTION OF TECHNICAL PROGRESS

A. Hydroprocessing Microreactor Development

All the three flow microreactors are operational in a nearly continuous fashion. The first microreactor is being used to study the reactivities of various sulfur-compounds like dibenzothiophene and its various methyl derivatives. Reports have already been made on the relative reactivities of these compounds and the influence of the degree and position of substitution (by methyl group) on the dibenzothiophene skeleton on the hydrodesulfurization reactivity in previous quarterly reports. Co-Mo/γ-Al_2O_3, Ni-Mo/γ-Al_2O_3 and Ni-W/γ-Al_2O_3 catalysts have been used at various stages. The full reaction networks of dibenzothiophene and 4,6-dimethyldibenzothiophene have been matter of discussion in ninth and tenth quarterly reports respectively. The second microreactor continues to be used for the hydrodenitrogenation reactions occasionally.

The third microreactor is in regular use for the full kinetic studies of hydrodesulfurization of dibenzothiophene.

In this quarter the 300 cm^3 batch autoclave reactor has been used to study the reactivities (HDS) of several multi-ring aromatic sulfur-containing compounds like thiophene, benzothiophene, dibenzothiophene, benzonaphtho-thiophene, etc.

B. Catalytic Hydrodesulfurization

1. Experimental

During this quarter a series of kinetic experiments in the batch reactor was completed. The reactor used was a 300 cm^3 autoclave fitted with a magnetic drive stirrer. Reactants were thiophene (1 ring), benzothiophene (2 ring), dibenzothiophene (3 ring), and benzonaphthothiophene (4 ring). Reaction conditions were identical for each reactant except for the weight of catalyst which was adjusted according to the reactivity of the sulfur compound toward desulfurization. The experimental conditions were:

- Catalyst: Co-Mo/γ-Al_2O_3 (HDS 16A), 149-178 μm partial size, 0.08-1.2 g
- Catalyst pretreatment: Sulfided externally at 400°C for 2 h with a constant flow of 10% H_2S in H_2 of 50 cm^3/min
- Reaction temperature: 300 ± 2°C
- Hydrogen Pressure: 70 ± 2 atm
- Reactant concentration: 0.25 mole % in n-hexadecane
- Volume of reactant mixture: 250 cm^3

2. Analysis

All analyses for reactant and product concentrations were carried out with a gas chromatograph equipped with flame ionization detector. A 3.4 m x .32 cm stainless steel column packed with 3% SP 2100 DB (Supelco methyl silicone with basic sites deactivated) on 100-120 mesh Supelcoport was used for all reactant and product analysis; the column was operated at various temperatures (i.e., from 140°-210°C depending on the reactant).

3. Results and Discussion

The hydrodesulfurization reactions under nearly identical experimental conditions have been reported (Houalla, 1978) to involve primarily the extrusion of sulfur accompanied by a small amount of aromatic ring hydrogenation before and after the sulfur removal step. This same behavior has been observed for the compounds studied here. Only in the case of benzonaphthothiophene has the hydrogenation of the aromatic rings been found to be at least as rapid as the hydrodesulfurization reaction. The major products of the hydrodesulfurization reaction for each sulfur compound are listed in Table 1.

In good agreement with the results of Wilson et al. (1957), Hoog (1950), Bartsch et al. (1974) and Ghosal et al. (1965,66), the hydrodesulfurization process has been found to follow pseudo first-order kinetics. The molar concentration of H_2 was at least 50 times higher than that of the sulfur compounds in the reactant mixture. So, even under the extreme conditions of total conversion of the sulfur-containing compound plus a minor amount of hydrogenation the concentration of H_2 concentration remained virtually constant. Under these conditions the rate of the hydrodesulfurization reaction can be represented by

$$r = k_1 C_s \qquad (1)$$

where r = rate
k_1 = pseudo first-order rate constant
C_s = concentration of sulfur-containing compound,

and the integrated rate equation (with respect to the batch reactor) is:

TABLE 1

COMPARISON OF THE PRODUCT DISTRIBUTION AND REACTIVITIES FOR THE HYDRODESULFURIZATION OF SEVERAL SULFUR-CONTAINING COMPOUNDS

Reactant	Major Products	Pseudo first-order rate Constant for Desulfurization K_1 cm^3/g cat hr	$\frac{K_1}{K_1 \text{ DBT}}$
1. 	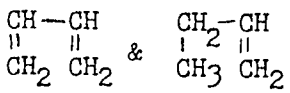	5,000	25.0
2. 	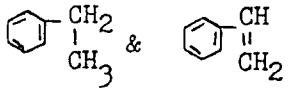	2,900	14.5
3. 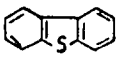	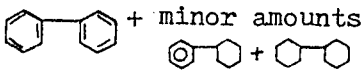	200	1.0
4. 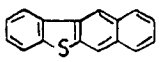	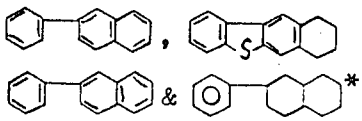	600	3.0
5. 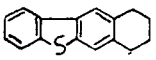	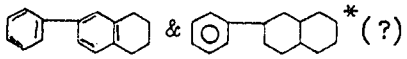	280	1.4

Reaction Conditions: Sulfided Co-Mo/γ-Al_2O_3 at 300°C. Batch Autoclave Reactor at 68 atm H_2 Pressure.

*This compound has not yet been identified beyond doubt.

$$- \ln (1-X) = k_1 \frac{W}{V} \cdot t \qquad (2)$$

where X = fractional conversion

W = mass of catalyst gm

V = average volume of solution, cm^3

t = time of reaction, hr.

k_1 = pseudo first-order rate constant, cm^3/gm catal. hr.

Figure 1 demonstrates the application of this rate equation for the five sulfur-containing compounds studied. Although thiophene and benzothiophene are well studied compounds they were included in our studies in order to get unambiguous data for direct comparison of the reactivities of all compounds in the series.

The data of our investigation have been compiled and are shown in Table 1. The pseudo first-order rate constants reflect the ease with which sulfur is removed as H_2S from the respective compounds. The third and fourth columns of Table 1 show that dibenzothiophene (a compound with 3 rings) is the least reactive compound. Table 1 also shows that the reactivities of the sulfur compounds decrease with increasing number of rings up to 3-ring compounds, and then the reactivity again increases with increasing number of rings.

Unlike the general observations with partially hydrogenated sulfur-containing compounds like tetra- and hexa-hydro dibenzothiophenes (Houalla, 1978), the reactivity of partially hydrogenated benzonaphthothiophene (i.e., tetrahydro benzonaphthothiophene) is much lower than that of benzonaphthothiophene itself. Therefore, it appears from the above observations that in the hydrodesulfurization process, the reactivities of multi-ring sulfur-containing compounds are not solely governed by their bulkiness.

The conclusions of this work are:

- Of all the well-known thiophene type of sulfur-containing compounds found in coal-derived liquids, dibenzothiophene and methyl dibenzothiophenes are the least reactive.
- The reactivity of aromatic sulfur-containing compounds decreases with the total number of rings present in the molecule, it reaches a minimum with 3-ring sulfur-containing compounds such as dibenzothiophene, and it increases for 4-ring sulfur-containing compounds such as benzonaphthothiophene.

C. Catalytic Hydrodenitrogenation

a. Binary Interactions

Determination of reaction network and detailed reaction kinetics in catalytic hydroprocessing reaction of a single nitrogen- or sulfur-containing compound has been of central focus in all the earlier quarterly reports. In industrial feeds nitrogen- and sulfur-containing compounds are present together with aromatics and studies of interactions of these compounds are of vital importance. Having valuable experience in dealing with complex reaction networks of single compounds, we have begun binary interaction studies. In the last quarterly report some preliminary results from this work were reported. Some detailed analysis and additional results are presented here.

(1) Hydrogenation of Naphthalene:

Hydrogenation of naphthalene was studied singly and in the presence of quinoline. Reaction conditions are listed in Table 2.

TABLE 2

Experimental Conditions

Temperature:	342°C
H_2 pressure:	500 psig
Catalyst:	Ni-Mo/γ-Al_2O_3 140-200 mesh sulfided for 2 hrs. at 400°C in the presence of 10% H_2S/H_2 (100 cc/min.)
CS_2 in feed:	0.05 wt %
Carrier oil:	Hexadecane
Naphthalene conc.:	$\sim 3.5 \times 10^{-4}$ gmole/g oil
Quinoline conc. (in binary reaction):	$\sim 3.5 \times 10^{-5}$ gmole/g oil (Naphthalene/quinoline ~10)

Naphthalene hydrogenates rapidly to tetralin which is further hydrogenated to two decalin isomers. The ratio of concentrations of trans-decalin and cis-decalin is constant over a period of 10 hr, suggesting that thermodynamic equilibrium exists with trans-decalin being the major product.

In the presence of quinoline, hydrogenation is strongly retarded (almost by a factor of 30) and decalins are produced in trace amounts. Time-concentration curves for reactants and products are given in Figs. 2, 3, and 4. Reaction network and comparison of rate constants with and without quinoline is presented in Table 3. Figs. 2 and 3 also indicate that time-concentration curves predicted from the model are in excellent agreement with experimental results. Formation of cis-decalin directly from tetralin (dotted root K_6) is possible but has not been evaluated.

(II) Hydrodesulfurization of Dibenzothiophene:

Hydrodesulfurization of dibenzothiophene was studied singly and in the presence of quinoline. Reaction conditions are the same as in Table 2, but the dibenzothiophene concentration is about $\sim 3.5 \times 10^{-5}$ gmole/g oil (DBT/Q = ~1).

Reaction network for dibenzothiophene hydrodesulfurization and comparison of the rate constants with and without quinoline is given below (Table 4). It is interesting to note that both direct removal of sulfur as well as hydrogenation is inhibited by quinoline but hydrogenation is retarded drastically and hydrodesulfurization reaction takes place via direct route of sulfur removal with formation of biphenyl in the presence of quinoline.

First order plots for disappearance of dibenzothiophene are given in Fig. 5. Time-concentration plots for reactant and intermediates are presented in Figs. 6 and 7.

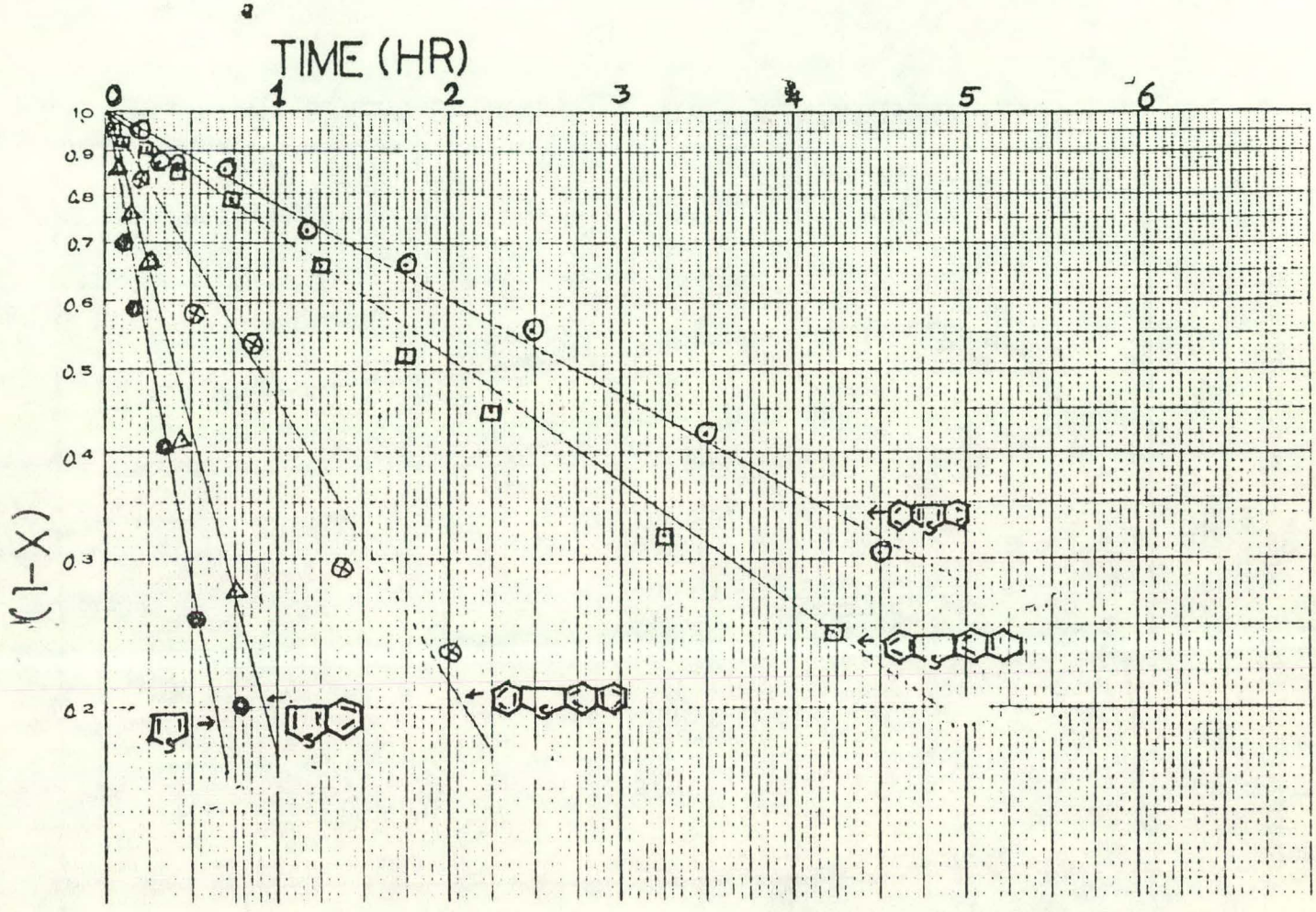

Figure 1: Pseudo first-order plots for the hydrodesulfurization of various sulfur compounds. Reaction conditions: Co-Mo/γ-Al_2O_3 (pre-sulfided at 400°C) T : 300 ± 2°C, Pressure: 68 ± 1 atm of H_2.

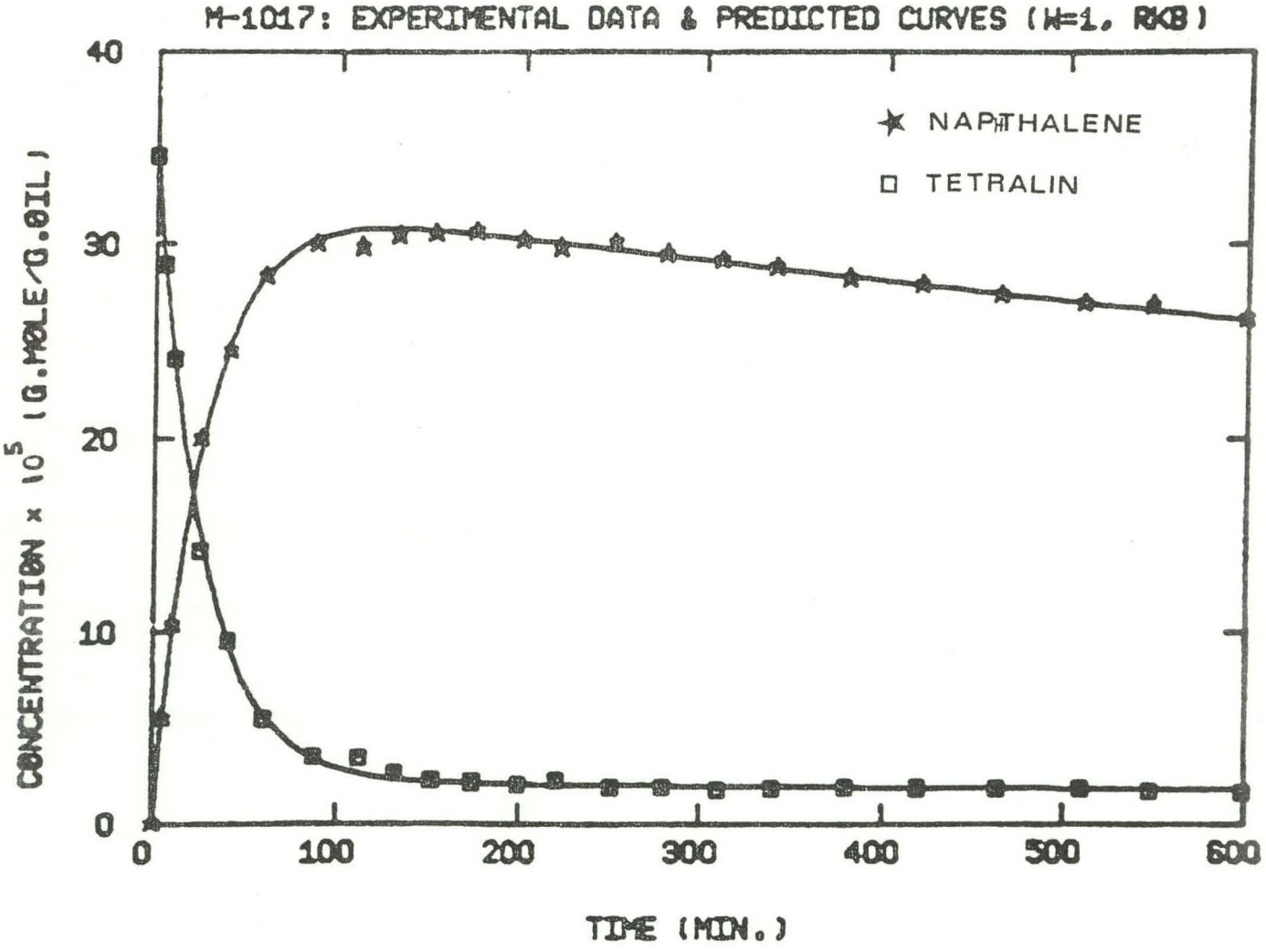

Figure 2: Concentration profiles of reactant naphthalene and tetralin (product) in catalytic hydrogenation of naphthalene. See text for experimental conditions.

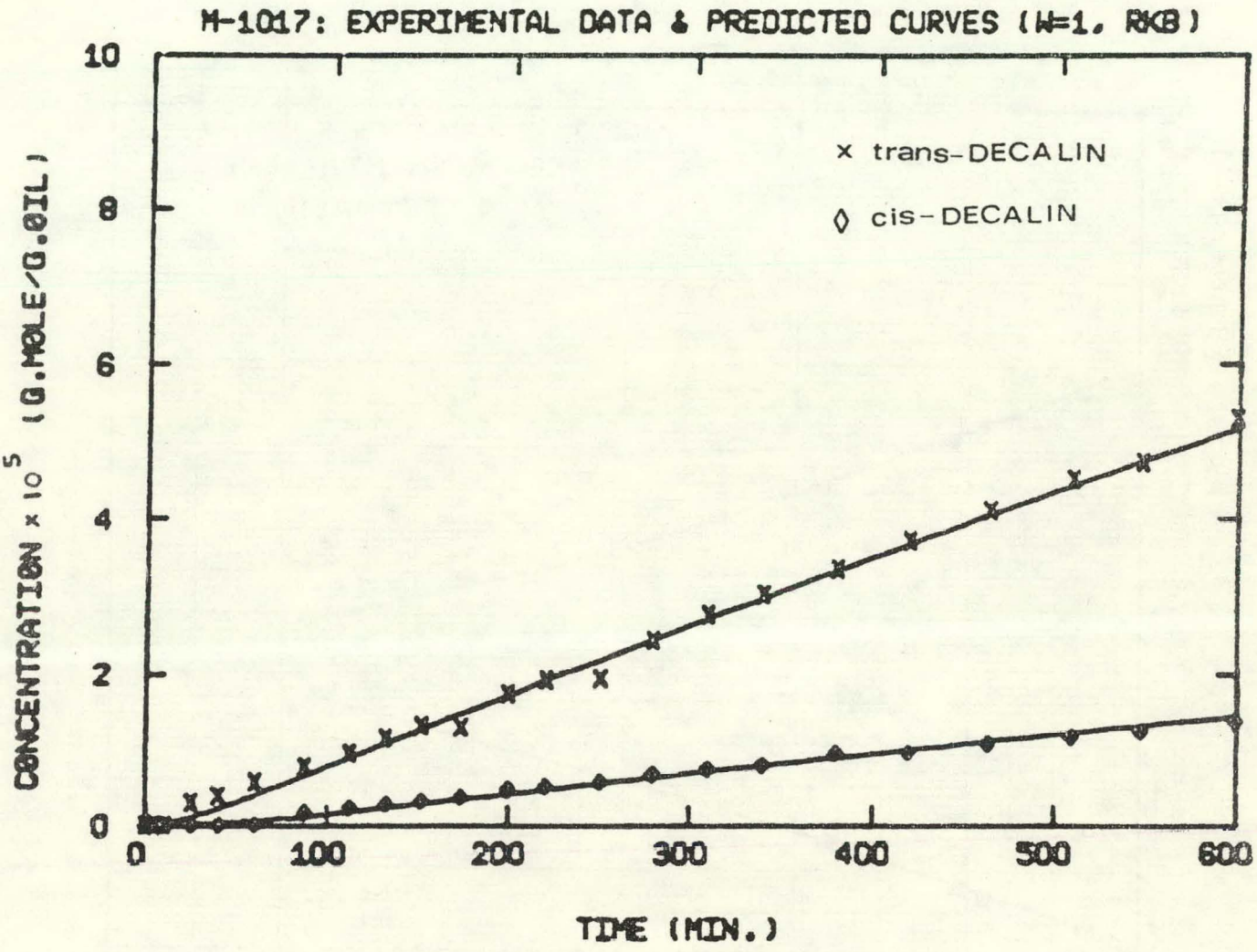

Figure 3: Concentration profiles of the hydrogenation products of naphthalene. See text for reaction conditions.

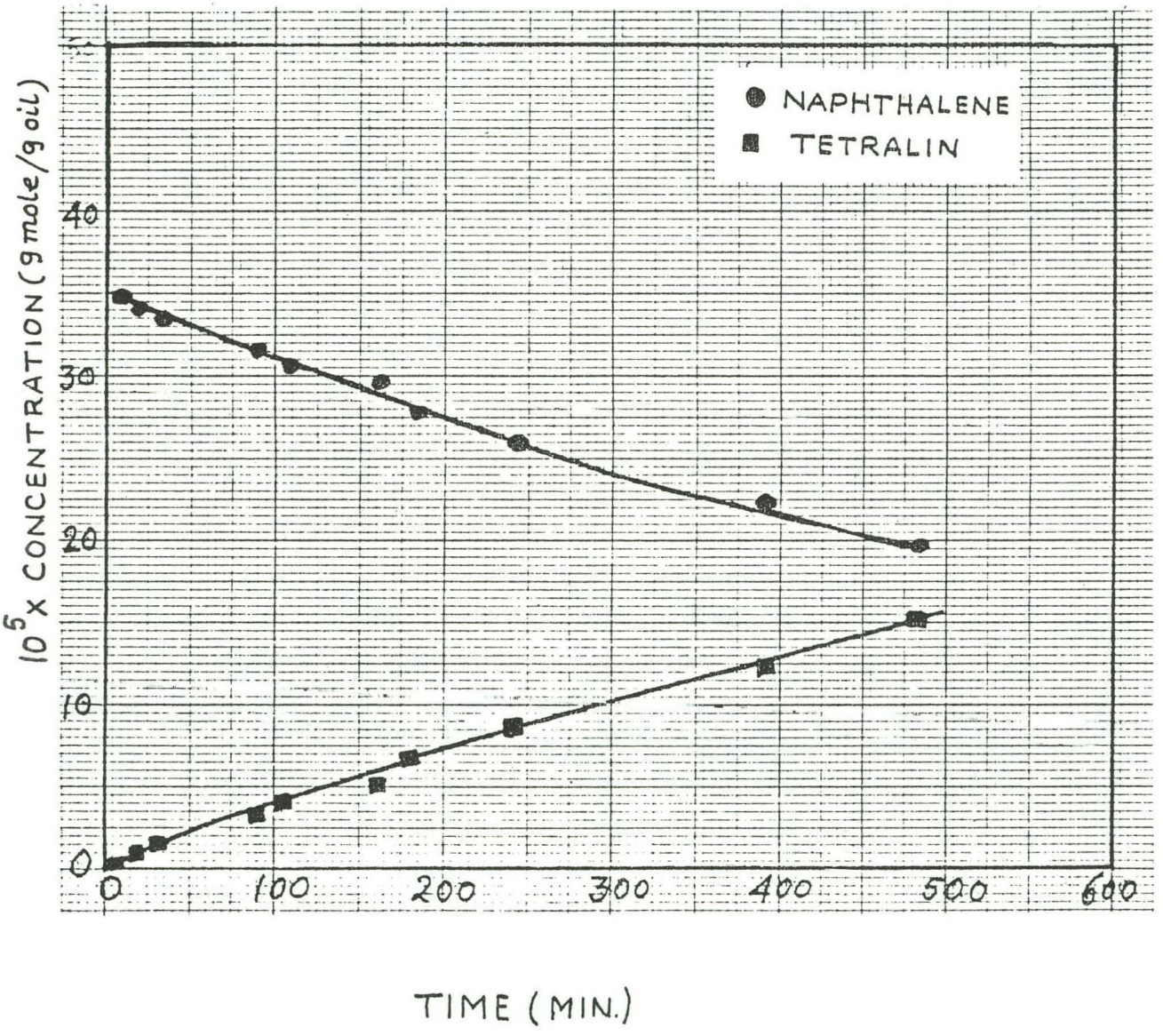

Figure 4: Concentration profiles of naphthalene (reactant) and tetralin (product) for the hydrogenation of naphthalene in presence of quinoline. See text for reaction conditions.

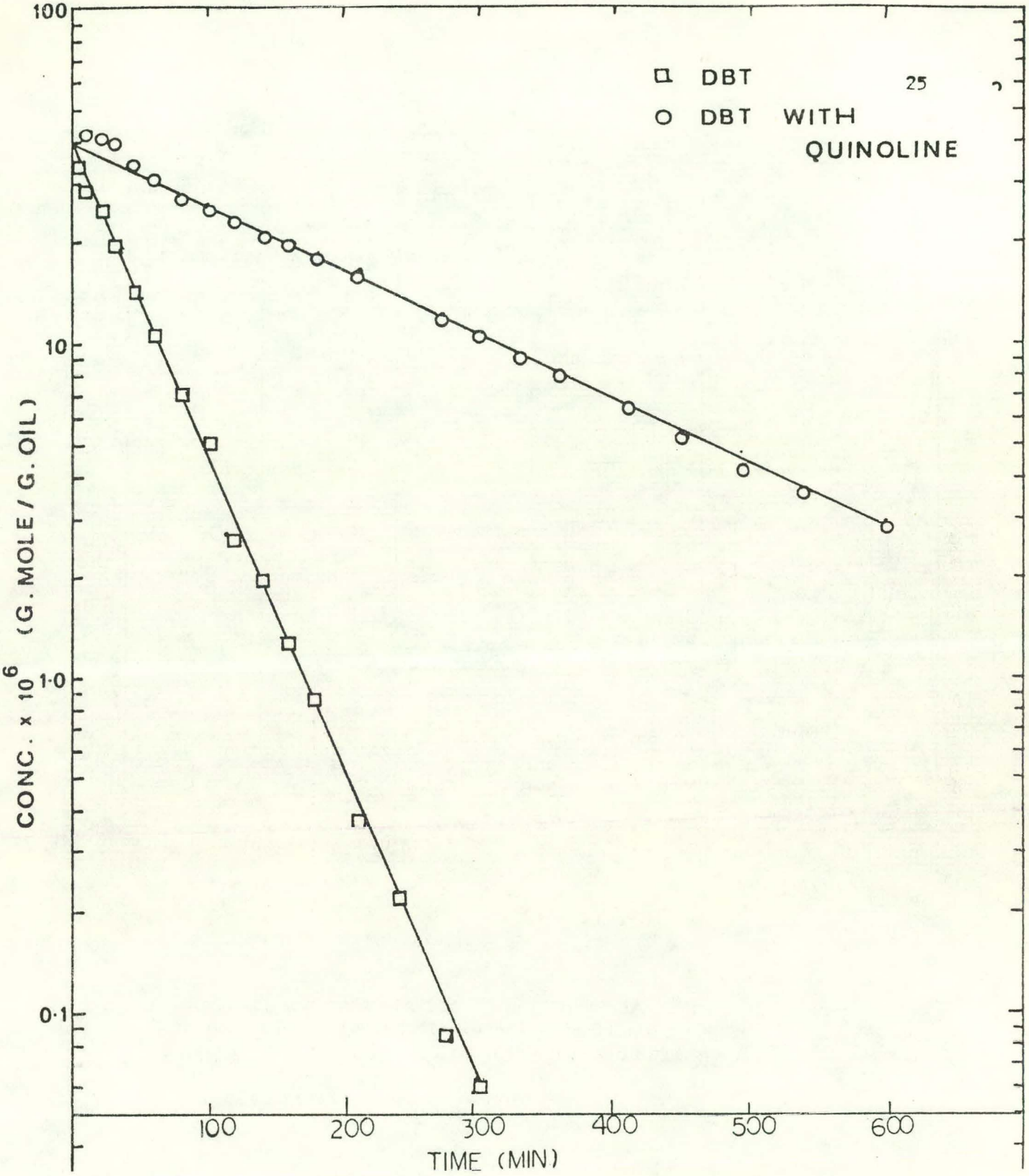

Figure 5: Pseudo first-order kinetics for the hydrodesulfurization of dibenzothiophene under two different conditions. Reaction conditions are given in the text.

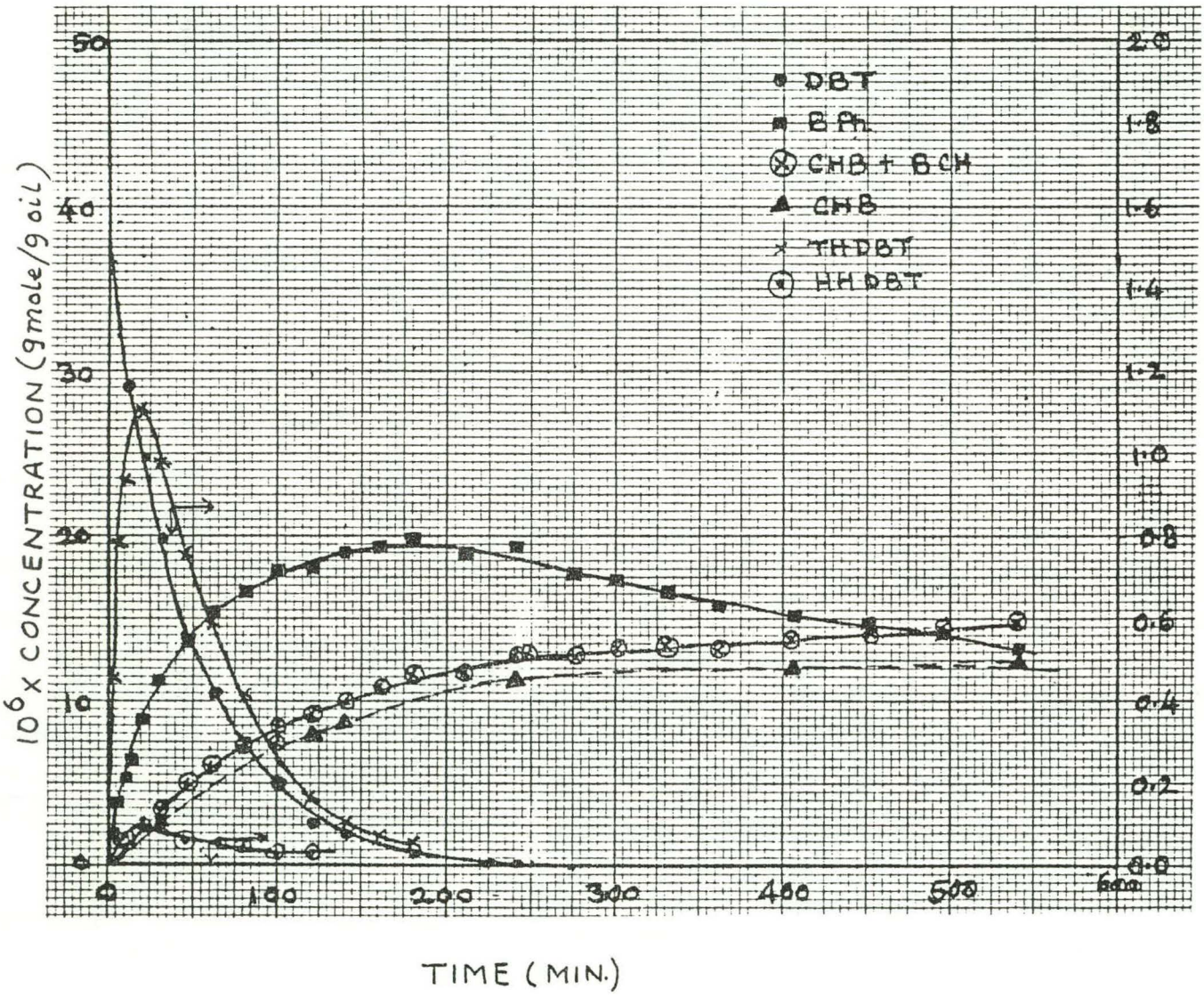

Figure 6: Concentration profiles of the reactant and products of hydrodesulfurization of dibenzothiophene. See text for the reaction conditions.

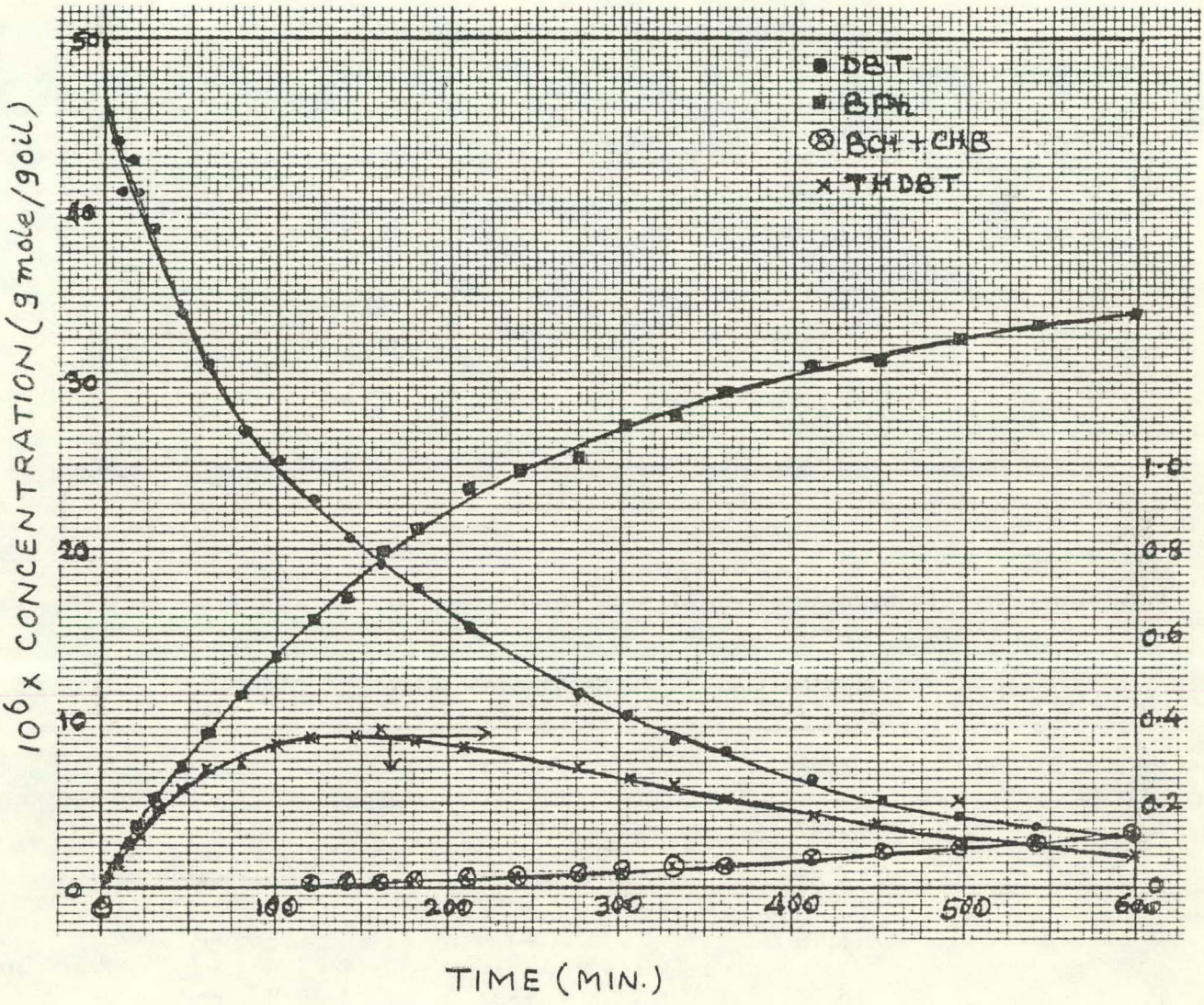

Figure 7: Concentration profiles of the reactant and products of hydrodesulfurization of dibenzothiophene in presence of quinoline. See text for reaction conditions.

TABLE 3

Proposed Reaction Network and Rate

Constants for Naphthalene Hydrogenation

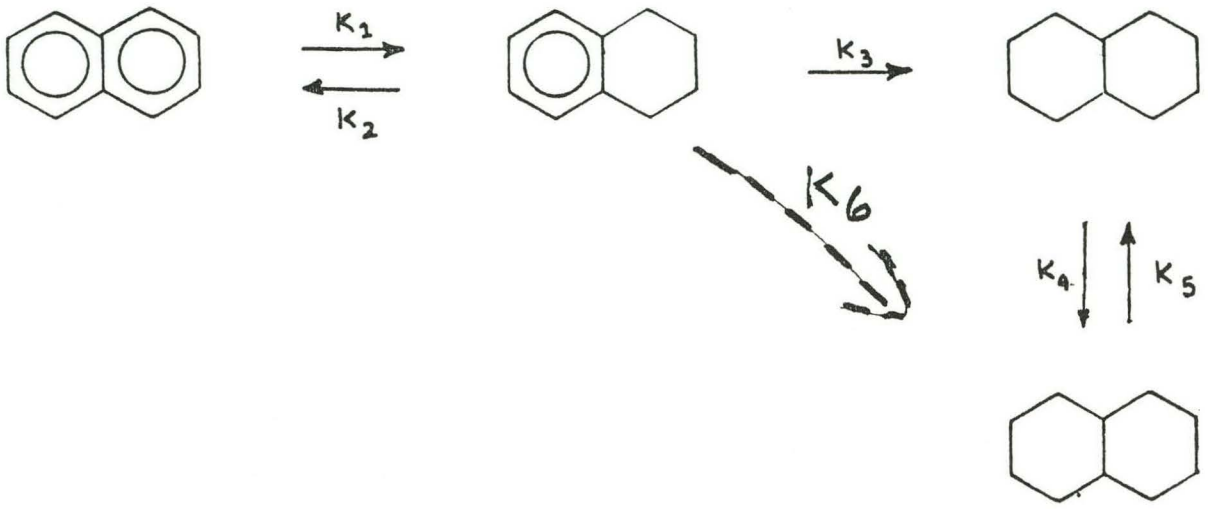

Rate constants* in hydrogenation of naphthalene.

	Naphthalene only (K)	Naphthalene with Quinoline (K')	K/K'
K_1	6.96	0.228	30.5
K_2	0.47	0	--
K_3	0.079	~0	--
K_4	1.76	--	--
K_5	5.98	--	--

*In units of g oil/g cat.-min, temp. 342°C, P: 500 psig H_2
carrier: n-hexadecane, 0.05 wt/CS_2, sulfided Ni-Mo/γ-Al_2O_3
Q/N ≃ 0.1

TABLE 4

Reaction Network and Rate Constants for

Dibenzothiophene Hydrodesulfurization

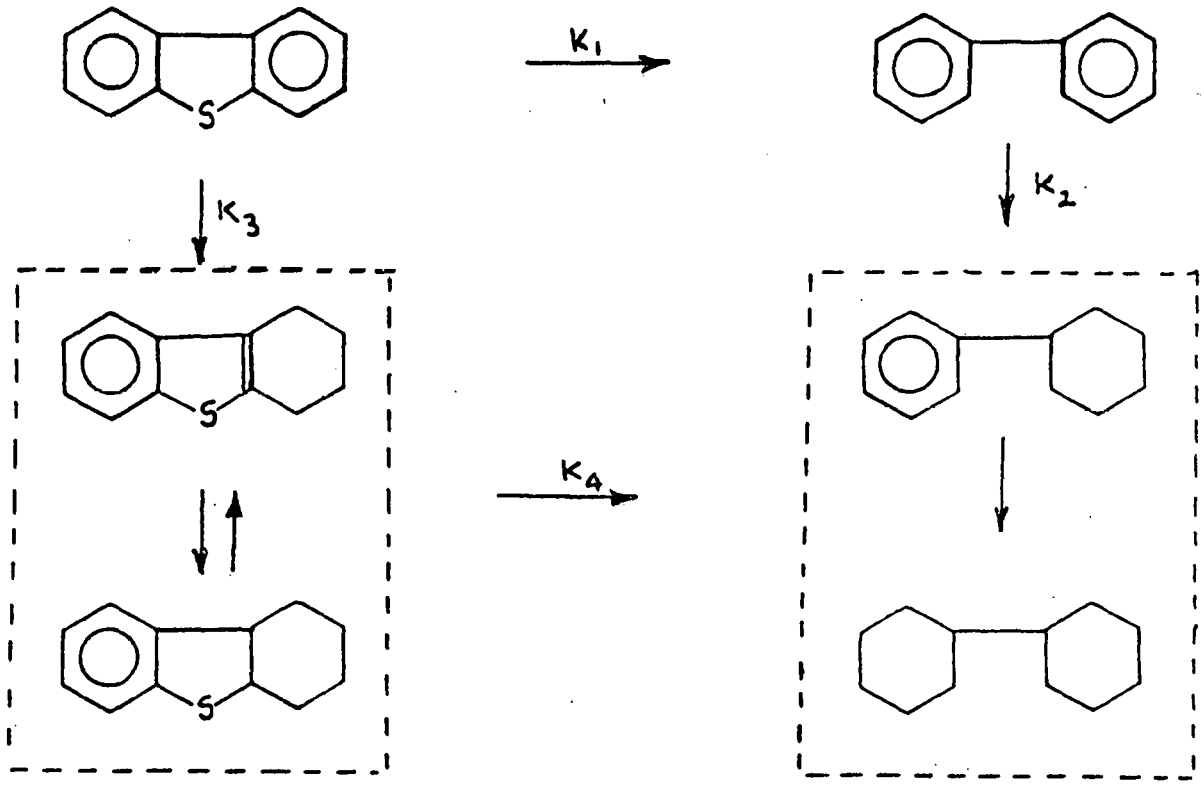

Rate constants* in hydrodesulfurization reaction network for dibenzothiophene

	DBT (only (K)	DBT with Quinoline (K')	K/K'
K_1	2.65	0.88	3.01
K_2	0.19	0.023	8.26
K_3	1.04	0.031	33.5
K_4	21.32	1.72	12.4
K_1+K_3	3.68	0.91	4.05

*In units of g oil/g cat-min.

342°C, 500 psig H_2, carrier C_{16}, 0.05 wt % CS_2, sulfided Ni-Mo/γ-Al_2O_3, Q/DBT ~1.

b. Hydrodenitrogenation of Benz[a]- and Dibenz[c,h]- acridines.

Analysis of results of hydrodenitrogenation of quinoline, acridine and benz[c] acridine showed that increase in number of benzene rings resulted in the decrease of hydrodenitrogenation reactivity. With this in mind, the following compounds were chosen for hydrodenitrogenation reactions

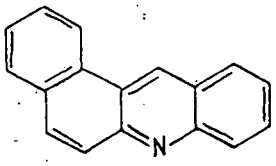

Benz[a]acridine
BA[a]

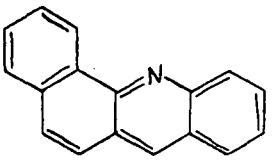

Benz[c]acridine
BA[c]

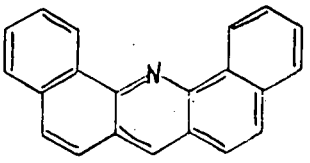

Dibenz[c,h]acridine
DBA[c,h]

Different reactivities of these compounds are expected because of the different environments of the nitrogen atom.

Experimental

Catalytic hydrodenitrogenation of Benz[a]acridine and dibenz[c,h]acridine was carried out in a 300 ml batch autoclave reactor. Operating conditions were:

- temperature: 367°C
- total pressure: 136 atm
- reactant concentration: 0.5 wt% in White Oil
- catalyst: Ni-Mo/γ-Al_2O_3 (HDS-9A) (140-200 mesh)
  0.5 wt% in carrier oil
  presulfided at 400°C in 10% H_2S for 2 hr
- CS_2 loading: 0.05 wt% (= 1.4 vol % H_2S in the gas phase)

Liquid samples were taken periodically and analyzed by a Perkin Elmer GC as described earlier in reports of this series.

Results

Our investigations reveal that the rates of conversion of benz[a]acridine and dibenz[c,h]acridine into hydrogenated nitrogen-containing compounds are very fast. During the initial period of reaction about 20 nitrogen compounds were generated which subsequently disappeared in a relatively short period of time. Figs. 8 and 9 show the concentration of total nitrogen as function of time. The same relationships are demonstrated in figures 10 and 11 for some (yet to be identified) nitrogen-containing products. To this time it has not been possible to unambiguously identify all of these intermediate nitrogen-containing compounds because their isolation by high-pressure liquid chromatography has not been entirely satisfactory. Further work on identification is underway and should be substantially completed in the next quarter.

The total rate of nitrogen removal from all nitrogen-containing compounds obeys pseudo first-order kinetics as shown in Figures 12 and 13. Table 5 summarized the reactivities of acridine derivatives for hydrodenitrogenation under the same experimental conditions.

TABLE 5

PSEUDO FIRST-ORDER RATE CONSTANTS FOR TOTAL NITROGEN REMOVAL FROM ACRIDINE DERIVATIVES

Compound	Rate Constant $\frac{\text{g oil}}{\text{min g cat}}$
Benz[a]acridine	1.08
Benz[c]acridine	1.54
Acridine	1.62
Dibenz[c,h]acridine	3.79

Reaction conditions: 367°C, 136 atm, sulfided Ni-Mo/γ-Al_2O_3, 0.5 wt % CS_2.

Once the total analysis is completed it will be possible to unravel the reaction network and explain the differences observed in reactivities. Investigations to this effect are in progress.

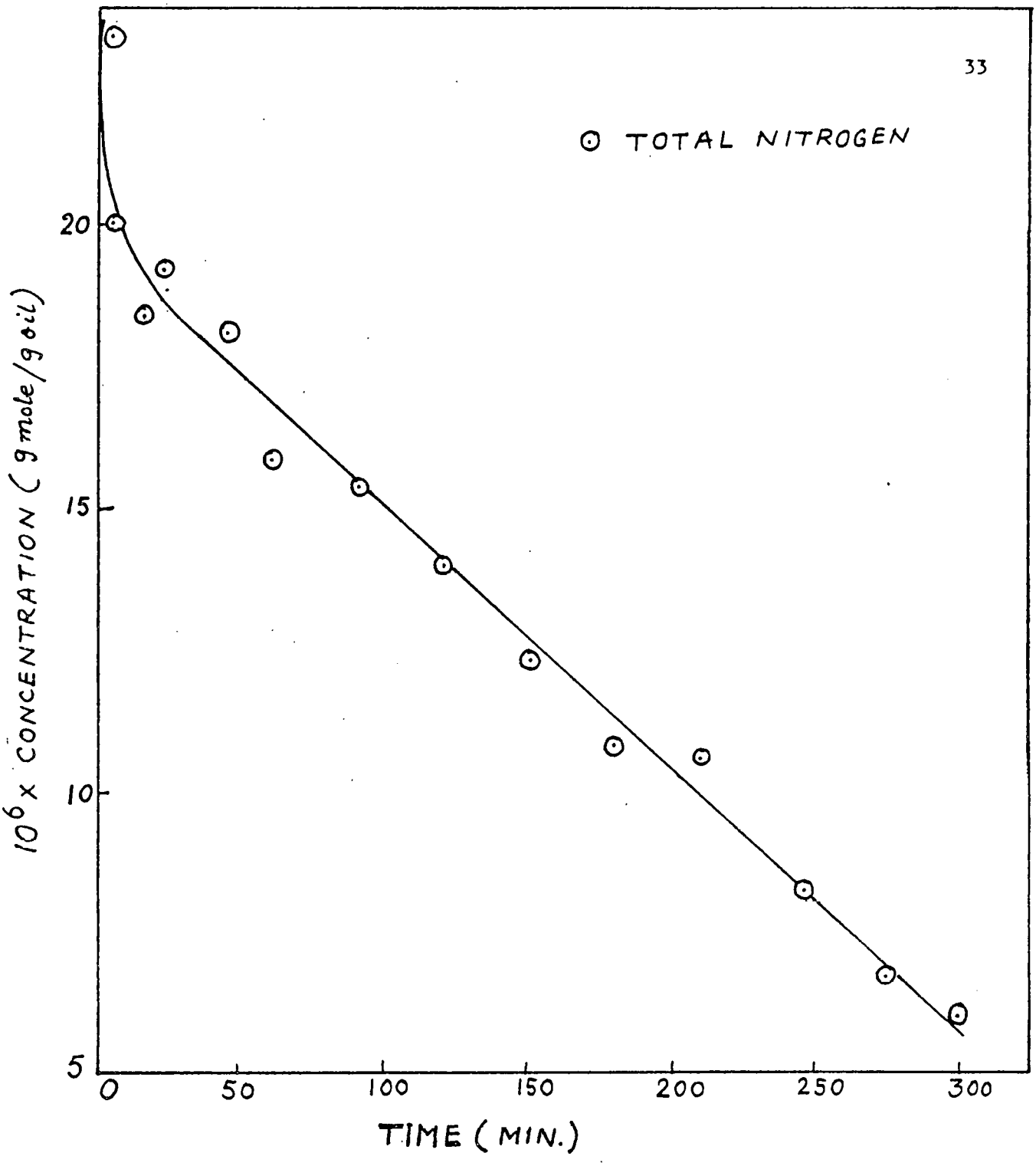

Figure 8: Concentration profile of benz[a]acridine during hydrodenitrogenation. Reaction conditions: Temp.: 367°C, Pressure: 2000 psig, Ni-Mo/γ-Al_2O_3 catalyst.

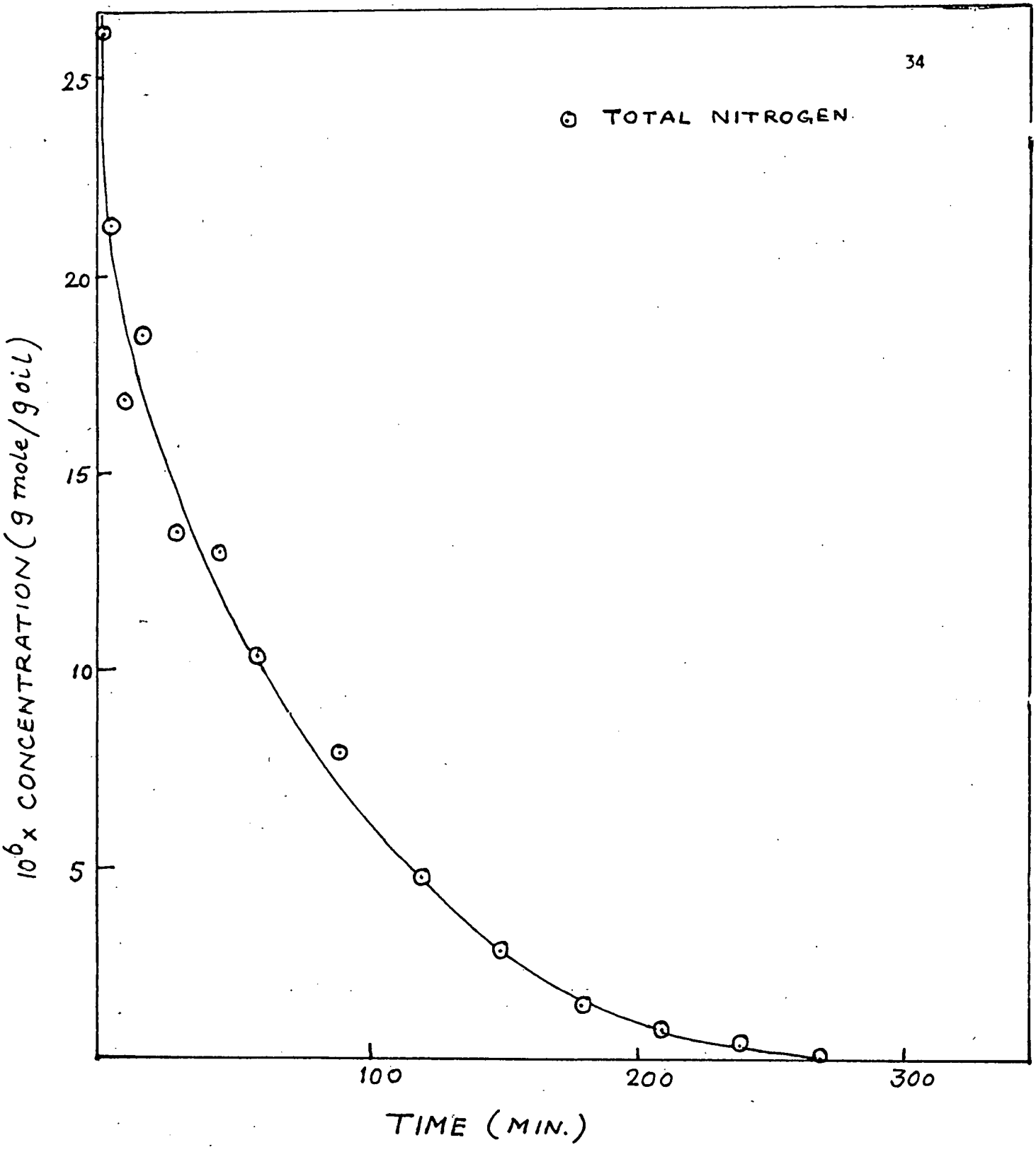

Figure 9: Concentration profile of dibenz[c,h]acridine during hydrodenitrogenation. Reaction conditions: Temp.: 367°C; Pressure: 200 psig, Ni-Mo/γ-Al_2O_3 catalyst.

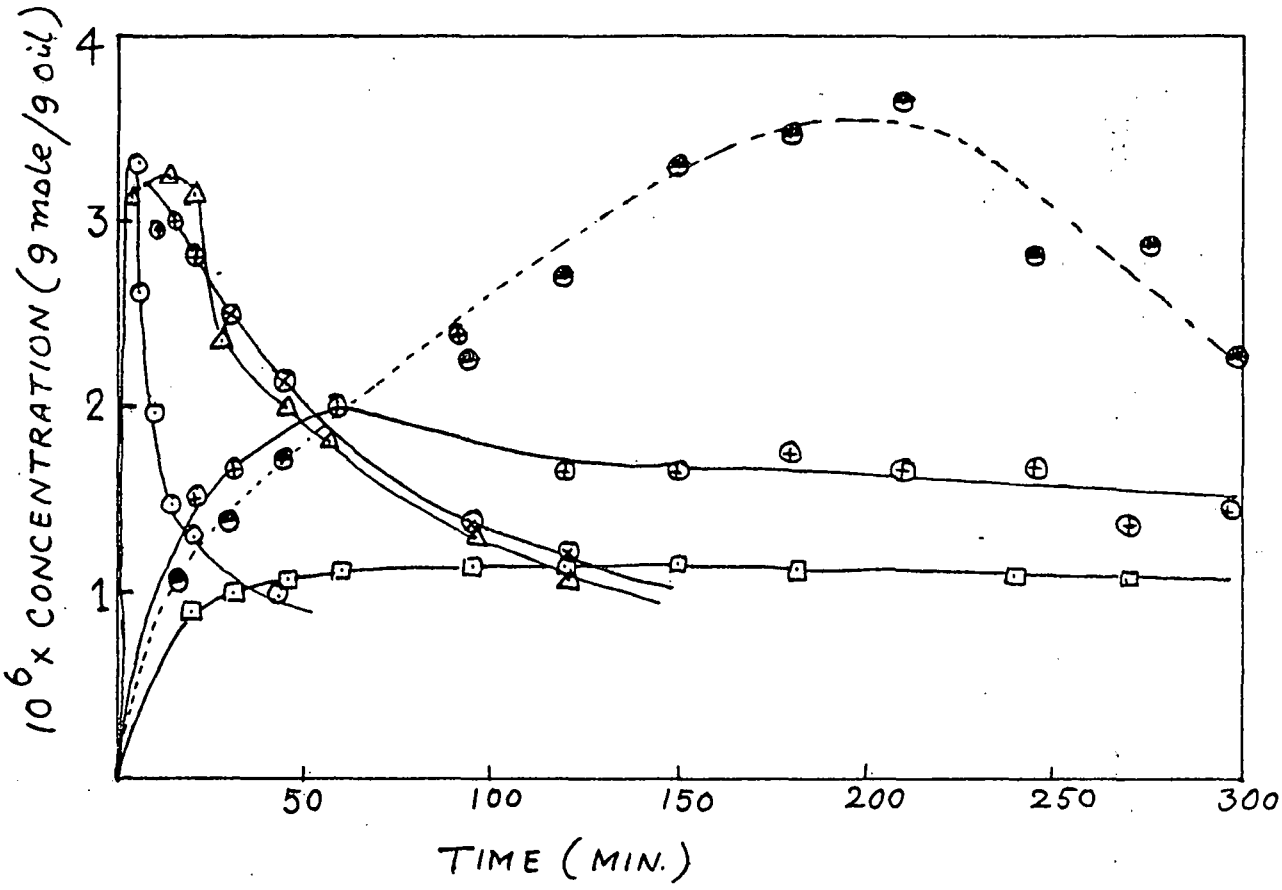

Figure 10: Concentration profiles of various hydrodenitrogenation products of benz[a]acridine. Reaction conditions: Temp.: 367°C, Pressure: 2000 psig, Ni-Mo/γ-Al_2O_3 catalyst.

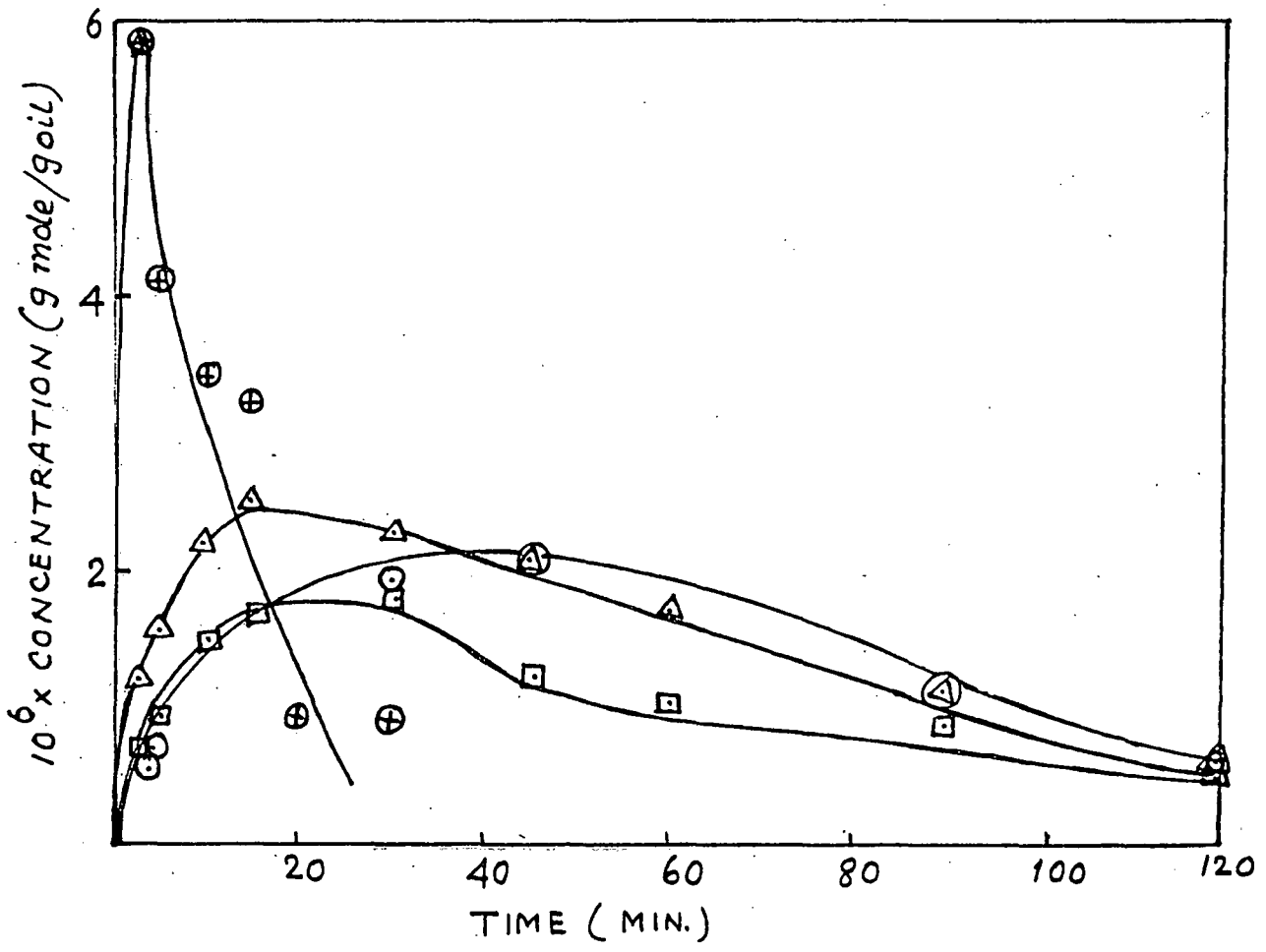

Figure 11: Concentration profiles of various hydrodenitrogenation products of dibenz[c,h]acridine. Reaction conditions: Temp.: 367°C, Pressure: 2000 psig, Ni-Mo/γ-Al_2O_3 catalyst. (The products are identified completely.)

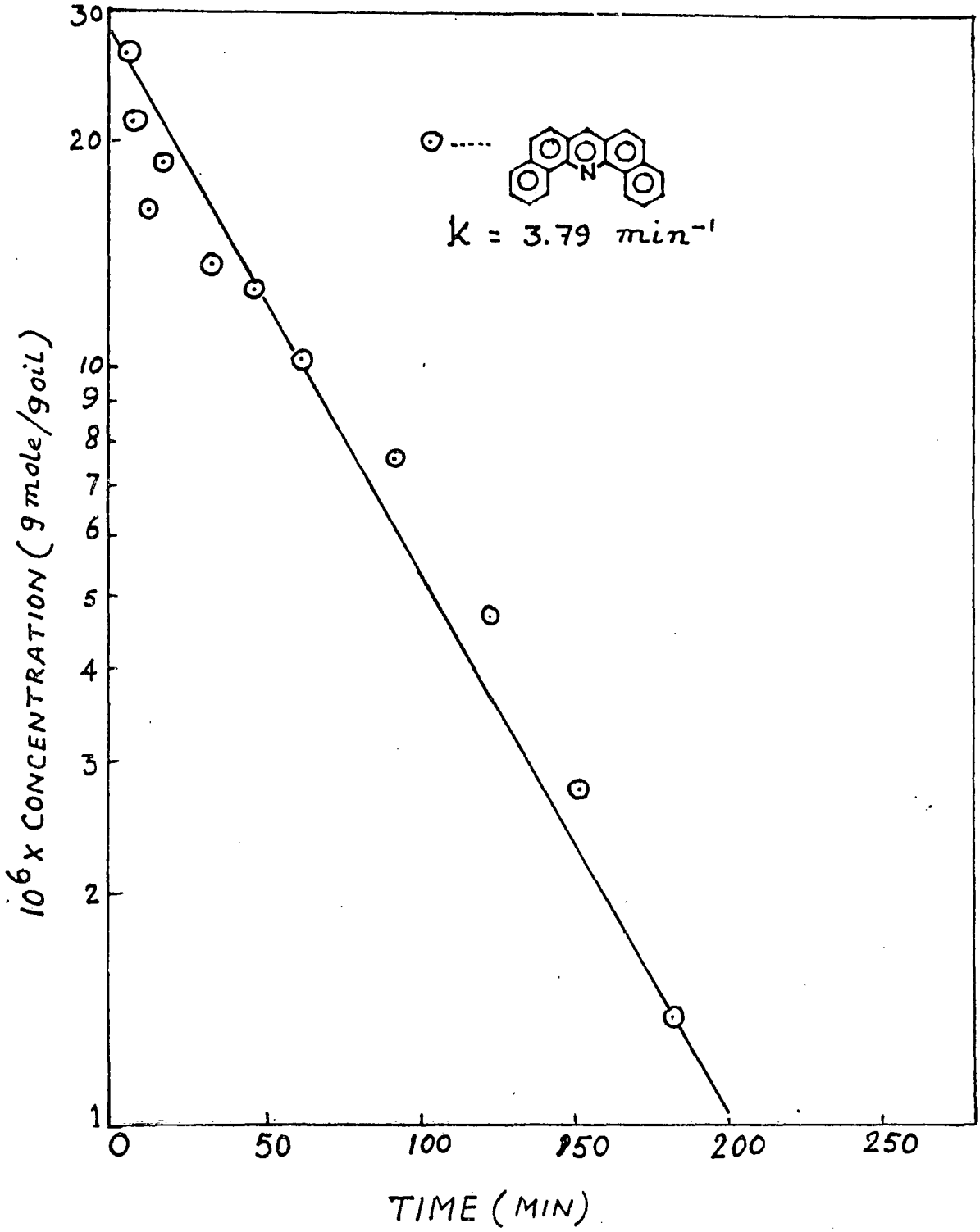

Figure 12: First order plot for total nitrogen removal from Dibenz[c,h]-acridine. Reaction conditions: Temp.: 367°C, Pressure: 2000 psig, Ni-Mo/γ-Al_2O_3 catalyst.

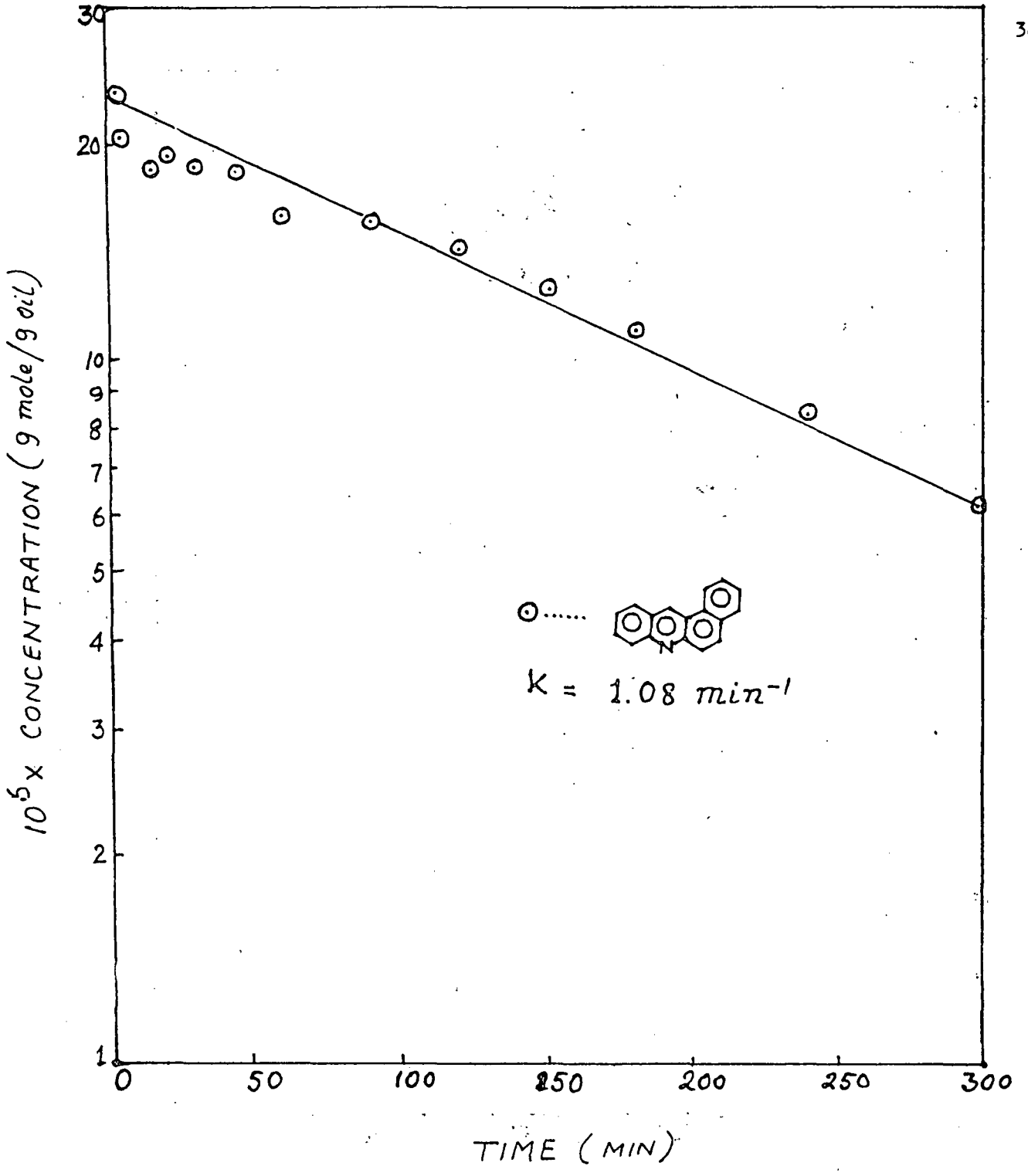

Figure 13: First order plot for total nitrogen removal from Benz[a]acridine. Reaction conditions: Temp.: 367°C, Pressure: 2000 psig, Ni-Mo/γ-Al_2O_3 catalyst.

D. Poisoning Reaction Engineering

In the last quarterly report, coking effects on the performance of H-coal® process were examined from the point of view of pore blockage caused by coke laydown and the effect of hindered diffusion of larger molecules in the partially closed pores. The results show that sometimes improvement in catalyst life and activity level can be obtained by proper selection of the pore size.

This report continues the studies of coking effects in the Synthoil process. In the previous studies of the physical properties of aged catalyst, it was reported that 50 to 70 percent of the pore volume had been lost for the catalyst samples from different sections of the reactor of the Synthoil process. It is believed that the volume of the catalyst particle lost is due to primarily the formation of coke during reaction and the sedimentation of coal matrix after the shut down of operation. A thorough understanding of the coke formations in the hydrotreating of coal liquids will lead to the elimination of coke formation and improvement of catalyst life.

Prototype mechanisms of series, parallel and independent mechanisms for coke formation were studied. Coke profiles, both in the fixed-bed reactor and inside the catalyst pellet, are predicted. The propagations of conversion and coke accumulation as a result of pore plugging and geometrical exclusion effects were investigated. These results will give insight into the basic aspects of coke formation, which will thus enable the more complex process to be characterized with a traceable phenomenon and promote better reactor design and catalyst life.

In the Synthoil process, hydrogen with a slurry of pulverized coal in a portion of product oil is introduced into a preheater before being fed to the catalytic fixed-bed reactor where the hydrotreating process takes place at the operating conditions of 450°C and 136 atm. Material balances characterizing the fluid phases both inside and outside the catalyst pellet for the specific reaction network in the fixed-bed reactor of Synthoil process are summarized in Tables 6 and 7 with appropriate boundary conditions. The implicit assumption made in formulation for these tables is that the time constant for the deterioration of the catalyst is relatively longer than that of residence and reactions, therefore, quasi-steady state can be assumed. At the same time, it is assumed that excess hydrogen is available from dissolved molecular liquid phase and also from the donor solvent. Consequently, the potential exterior mass-transfer limitation will be at the liquid-solid interface. The criteria and theoretical model to describe the general phenomenon of coke formations are similar to that developed for the H-coal process. Therefore, only the qualitative results are discussed.

For the sake of demonstrating the effect of coke on the catalyst behavior in the fixed bed of the Synthoil process, typical exponents with $\alpha = \beta = \gamma = \delta = 1$ in the power-law reaction mechanism are considered. Some secondary parameters are assumed empirically as follows:

$$B_{o,i} = 50$$

$$\text{LHSV} = 0.5\ \text{hr}^{-1}$$

$$\text{Pec,i} = 2.0$$

$$\frac{d_p}{L} = .02$$

$$\xi_b = .04$$

Table 6 : Dimensional Material Balances for Synthoil Process

	$c \xrightarrow{1} b$, $c \xrightarrow{2} \bar{p}$	$c \xrightarrow{1} b \xrightarrow{2} \bar{p}$	$c \xrightarrow[2]{1} b$, $p \xrightarrow{} \bar{p}$
For Reactor Bed :			
$D_{a,1}\frac{\partial^2 c}{\partial x^2} - v\frac{\partial c}{\partial x} - \frac{K_{f,1}\cdot S}{\xi_b}(c-\tilde{c}_s) =$	0	0	0
$D_{a,2}\frac{\partial^2 y}{\partial x^2} - v\frac{\partial y}{\partial x} - \frac{K_{f,2}\cdot S}{\xi_b}(y-\tilde{y}_s) =$	———	0	0
B.C. $-D_{a,1}\frac{\partial c}{\partial x}\Big\vert_{x=0^+} =$	$v(c\vert_{x=0^-} - c\vert_{x=0^+})$	$v(c\vert_{x=0^-} - c\vert_{x=0^+})$	$v(c\vert_{x=0^-} - c\vert_{x=0^+})$
$-D_{a,2}\frac{\partial y}{\partial x}\Big\vert_{x=0^+} =$	———	0	$v(p\vert_{x=0^-} - p\vert_{x=0^+})$
$\frac{\partial c}{\partial x}\Big\vert_{x=L} =$	0	0	0
$\frac{\partial y}{\partial x}\Big\vert_{x=L} =$	———	0	0
For Catalyst Pellet :			
$\frac{1}{r^2}\left(\frac{\partial}{\partial r}(r^2 D_{e,1}\frac{\partial \tilde{c}}{\partial r}\right) =$	$k_1\theta^\alpha\tilde{c}^\beta + k_2\theta^\delta\tilde{c}^\gamma$	$k_1\theta^\alpha\tilde{c}^\beta$	$k_1\theta^\alpha\tilde{c}^\beta$
$\frac{1}{r^2}\left(\frac{\partial}{\partial r}(r^2 D_{e,2}\frac{\partial \tilde{y}}{\partial r}\right) =$	———	$k_2\theta^\delta\tilde{b}^\gamma - k_1\theta^\alpha\tilde{c}^\beta$	$k_2\theta^\delta\tilde{p}^\gamma$
$\frac{\partial \bar{b}}{\partial t} =$	$k_2\theta^\delta\tilde{c}^\gamma$	$k_2\theta^\delta\tilde{b}^\gamma$	$k_2\theta^\delta\tilde{p}^\gamma$
I.C. $\bar{p}(t=0) =$	0	0	0
B.C. $\frac{\partial \tilde{c}}{\partial r}\Big\vert_{r=0} =$	0	0	0
$\frac{\partial \tilde{y}}{\partial r}\Big\vert_{r=0} =$	0	0	0
$D_{e,1}\frac{\partial \tilde{c}}{\partial r}\Big\vert_{r=r_p} =$	$K_{f,1}(c-\tilde{c}_s)$	$K_{f,1}(c-\tilde{c}_s)$	$K_{f,1}(c-\tilde{c}_s)$
$D_{e,2}\frac{\partial \tilde{y}}{\partial r}\Big\vert_{r=r_p} =$	———	$K_{f,2}(b-\tilde{b}_s)$	$K_{f,2}(p-\tilde{p}_s)$

Table 7 : Dimensionless Material Balances for Synthoil Process

	$C \xrightarrow{1} B$, $C \xrightarrow{2} \bar{p}$	$C \xrightarrow{1} B \xrightarrow{2} \bar{p}$	$C \xrightarrow{1} \underline{B}$, $P \xrightarrow{2} \underline{P}$
For Reactor Bed :			
$\Psi_1 \frac{\partial^2 C}{\partial X^2} - \frac{\partial C}{\partial X} - \Theta_1(C-\tilde{C}_s) =$	0	0	0
$\Psi_2 \frac{\partial^2 Y}{\partial X^2} - \frac{\partial Y}{\partial X} - \Theta_2(Y-\tilde{Y}_s) =$	———	0	0
B.C.			
$-\Psi_1 \frac{\partial C}{\partial X}\Big\vert_{X=0^+} =$	$1 - C$	$1 - C$	$1 - C$
$-\Psi_2 \frac{\partial Y}{\partial X}\Big\vert_{X=0^+} =$	———	0	$1 - P$
$\frac{\partial C}{\partial X}\Big\vert_{X=1} =$	0	0	0
$\frac{\partial Y}{\partial X}\Big\vert_{X=1} =$	———	0	0
For Catalyst Pellet :			
$Cd,1\, \nabla^2 \tilde{C} + \frac{\partial Cd,1}{\partial f} \cdot \frac{\partial \tilde{C}}{\partial f} =$	$\phi_1^2 \theta^\alpha \tilde{C}^\beta + \phi_2^2 \theta^\delta \tilde{C}^\gamma$	$\phi_1^2 \theta^\alpha \tilde{C}^\beta$	$\phi_1^2 \theta^\alpha \tilde{C}^\beta$
$Cd,2\, \nabla^2 \tilde{Y} + \frac{\partial Cd,2}{\partial f} \cdot \frac{\partial \tilde{Y}}{\partial f} =$	———	$\phi_2^2 \theta^\delta \tilde{B}^\gamma - \phi_1^2 \theta^\alpha \tilde{C}^\beta$	$\phi_2^2 \theta^\delta \tilde{P}^\gamma$
$\frac{\partial \theta}{\partial \tau} =$	$- \theta^\delta \tilde{C}^\gamma$	$- \theta^\delta \tilde{B}^\gamma$	$- \theta^\delta \tilde{P}^\gamma$
I.C. $\theta(\tau=0) =$	1	1	1
B.C.			
$\frac{\partial \tilde{C}}{\partial f}\Big\vert_{f=0} =$	0	0	0
$\frac{\partial \tilde{Y}}{\partial f}\Big\vert_{f=0} =$	———	0	0
$Cd,1 \frac{\partial \tilde{C}}{\partial f}\Big\vert_{f=1} =$	$B_{o,1}(C-\tilde{C}_s)$	$B_{o,1}(C-\tilde{C}_s)$	$B_{o,1}(C-\tilde{C}_s)$
$Cd,2 \frac{\partial \tilde{Y}}{\partial f}\Big\vert_{f=1} =$	———	$B_{o,2}(B-\tilde{B}_s)$	$B_{o,2}(P-\tilde{P}_s)$

where i = 1,2. The qualitative observation of the general phenomenon will be elucidated below.

Figs. 14 to 16 show the effect of pore plugging and geometric exclusion on the time change of conversion for parallel, series and independent mechanisms respectively. The upper parts show the effect of geometrical exclusion alone on the performance of the Synthoil process. While the results for parallel and independent mechanisms indicate that hindered diffusion effect is not significant for $\lambda_{o,i}$ less than 0.2, it appears rather important for the series mechanism. The lower parts of these figures show the combination effects of strong pore plugging and hindered diffusion. The importance of these effects will be apparent as $\lambda_{o,i}$ increases. The dashed line indicates that the conversion drops to zero due to the termination of catalyst life by complete pore blockage, even though the activity still remaining high in the interior of catalyst pellet.

Fig. 17 shows the prediction of coke profiles along the fixed-bed reactor. A sharp distribution from the entrance to the exit is observed for the parallel mechanism. As λ_o increases, the sharpness disappears, because the geometrical exclusion effect slows down the mass flux of the main reaction with higher Thiele modulus. Therefore, the activity remains uniform for coking reaction. The results for series and independent mechanisms appear quite uniform along the reactor for specific parameters concerned.

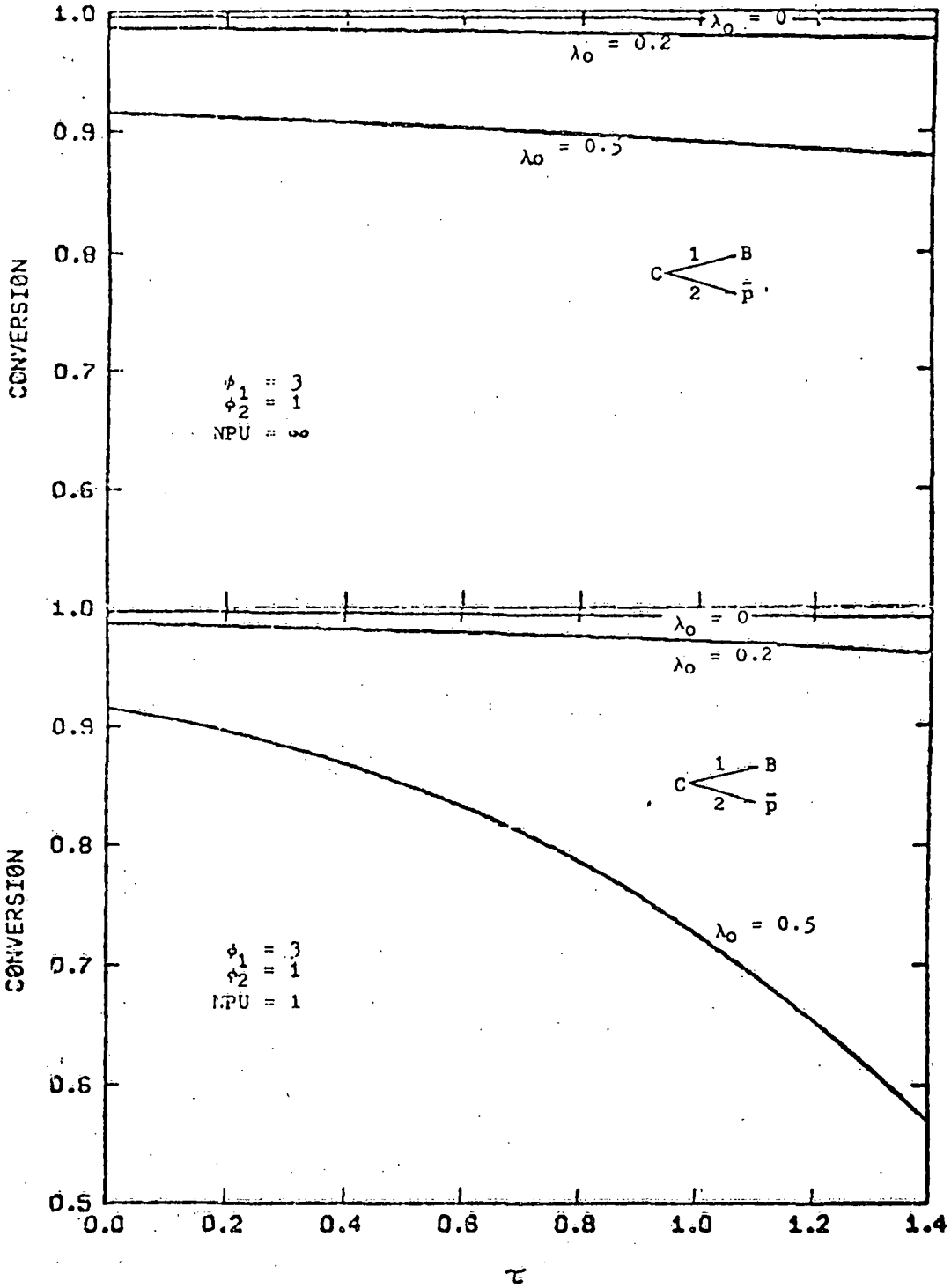

Fig. 14

Effects of pore plugging and geometrical exclusion on the time change of conversion for parallel mechanism.

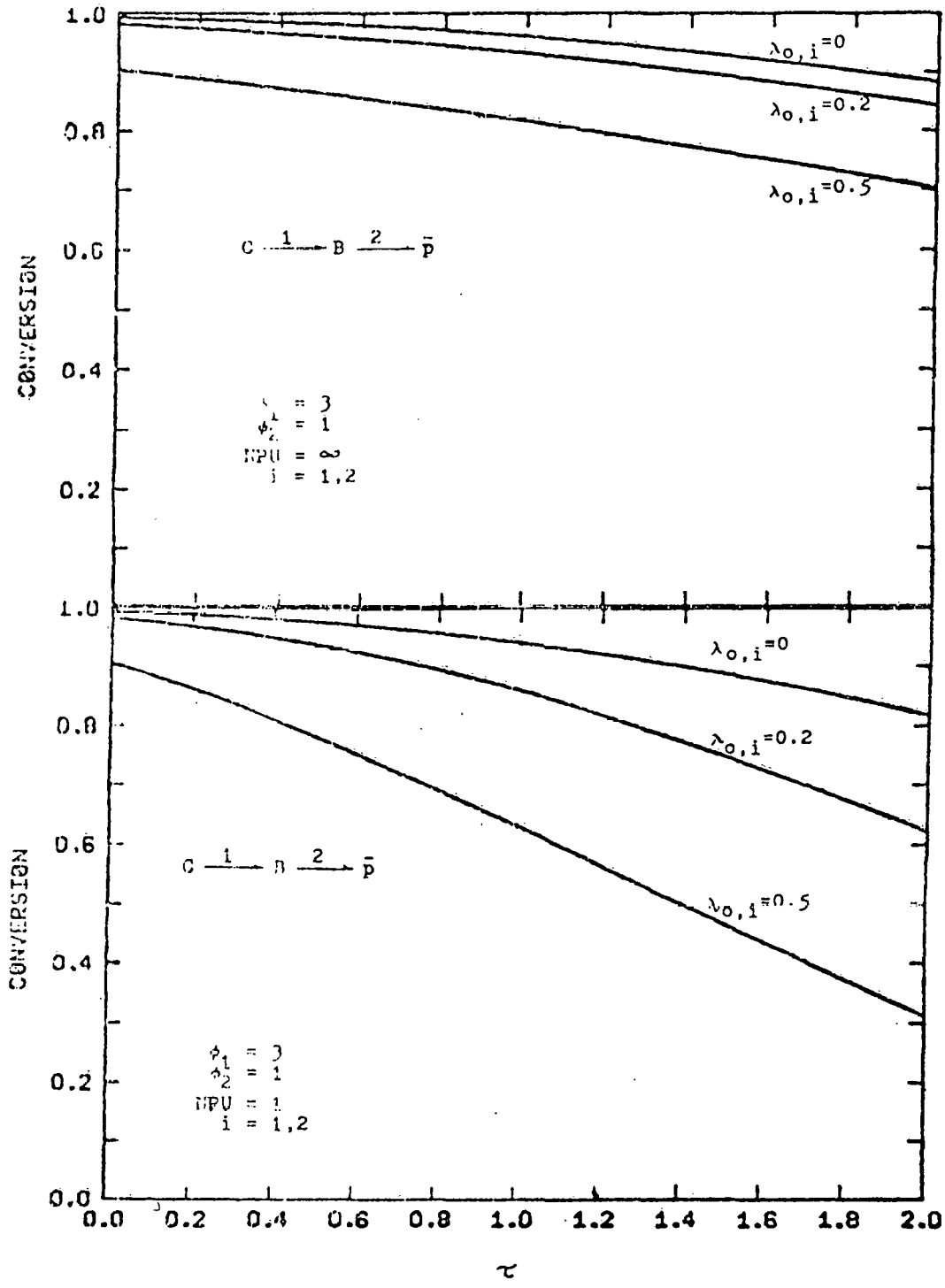

Fig. 15

Effect of pore plugging and geometrical exclusion on the time change on conversion for series mechanism.

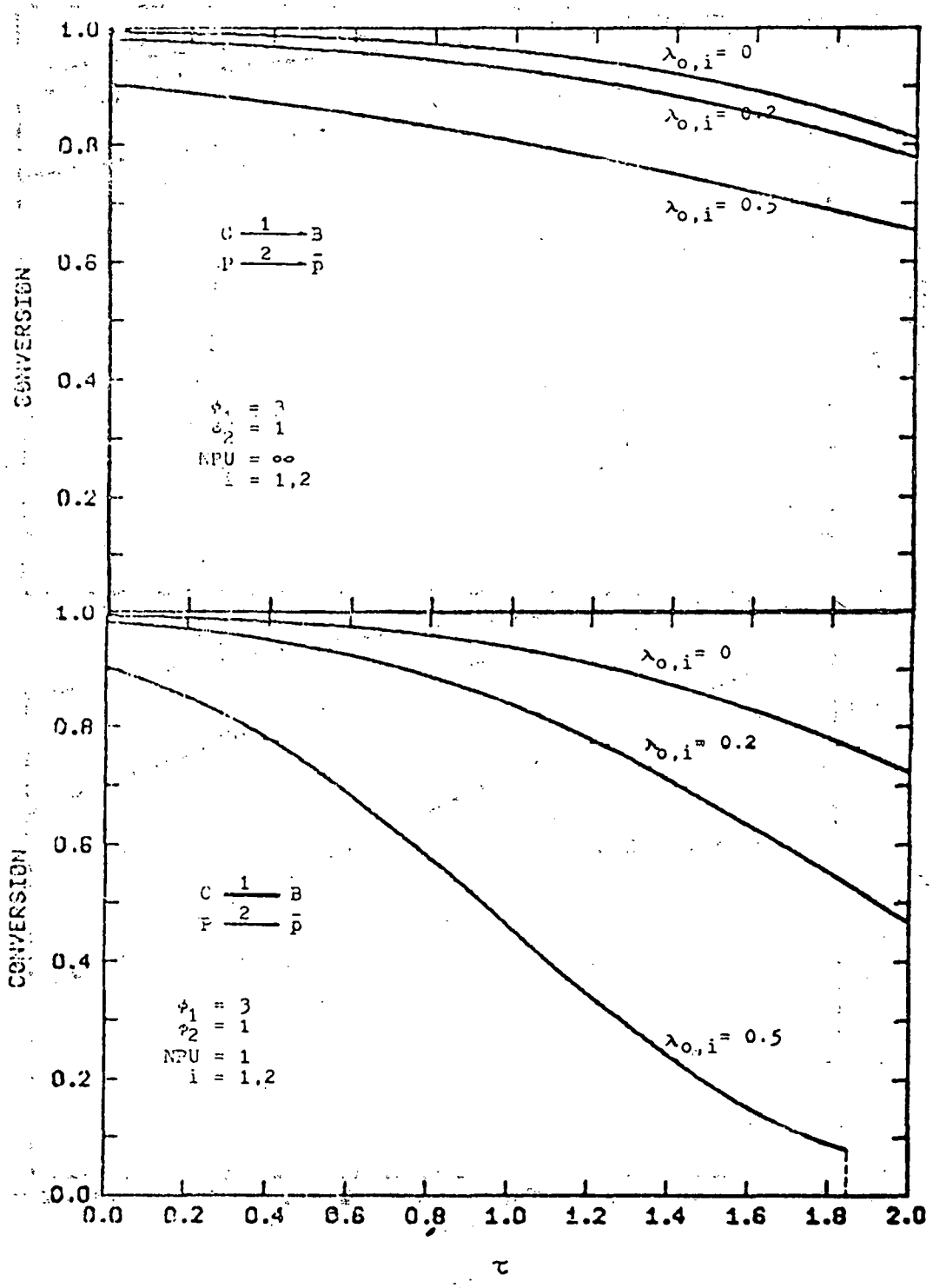

Fig. 16

Effect of pore plugging and geometrical exclusion on the time change of conversion for independent mechanism.

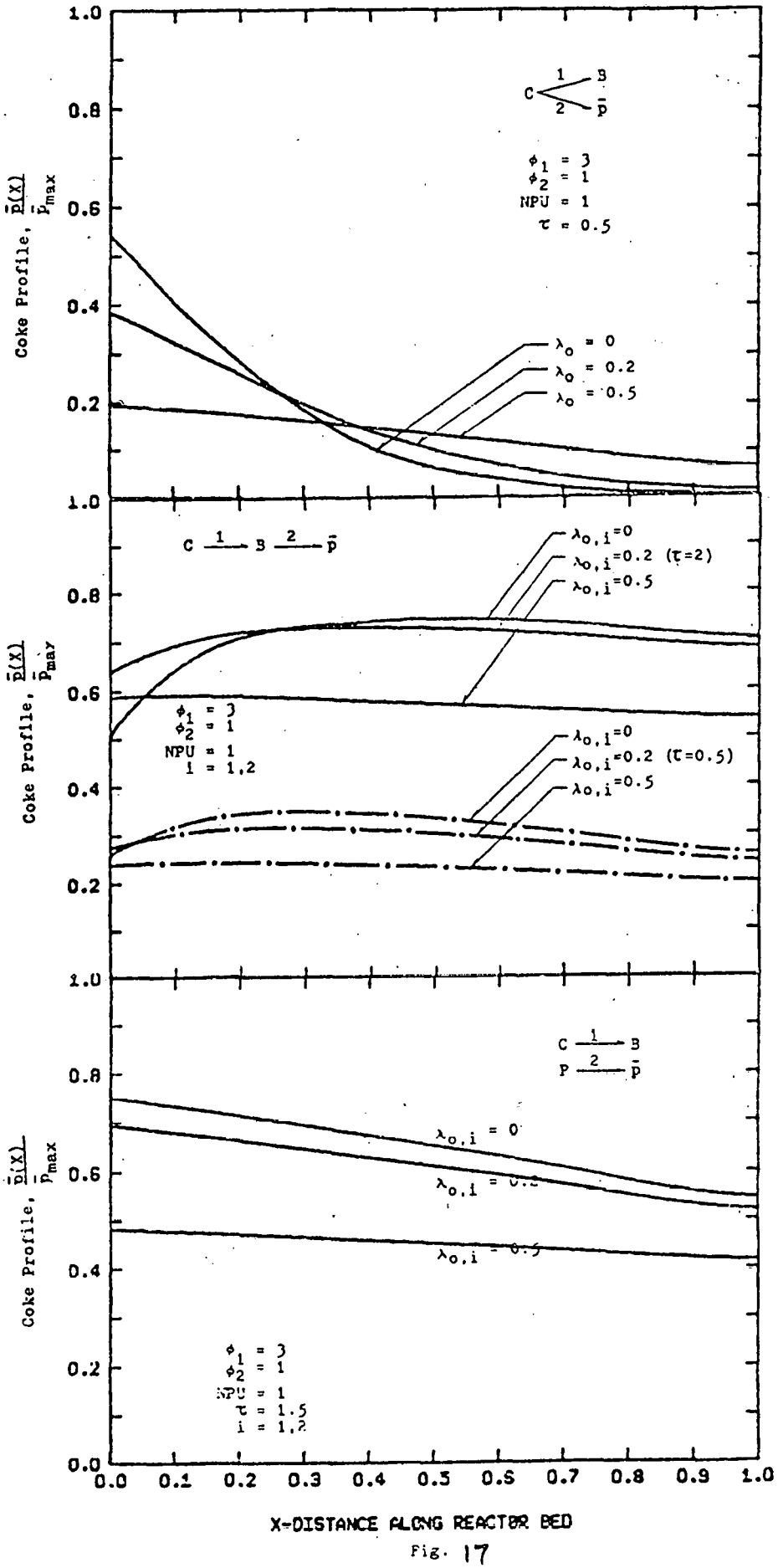

Fig. 17

Coke profiles along the fixed bed reactor as a function of $\lambda_{o,i}$ for parallel, series and independent mechanisms.

The coke profiles inside the catalyst pellet in different sections of the reactor were shown in Figures 18 to 20. The results of Figure 18 show that the distribution of coke profiles depends strongly on the location along the reactor and inside the catalyst pellet. The increase of the geometrical exclusion will result in the coke deposition in the outer shell of the catalyst pellet. The results of Figures 19 and 20 show that coke profiles are apparently uniform for series and independent mechanisms. The non-uniform distribution inside the catalyst pellet will occur when $\lambda_{o,i}$ is increased.

The comparison of accumulation of coke laydown is shown in Figure 21. For this typical set of parameters studied, the coke laydown decreases in the following order: series > independent > parallel. Little quantity of coke accumulation will be observed for the parallel mechanism. Physically, this low coke accumulation is due to the high competition of the main reaction. The coke build-up approaches steady-state relatively fast for the series mechanism. The dashed line indicates that coke build-up is terminated as the catalyst life is over. The termination of catalyst life depends strongly on the reaction networks and the geometrical exclusion effect.

From the above discussion, we demonstrate that physical properties of both catalyst and reacting molecules have a decisive effect on the catalyst deactivation and the nature of coke formation. These results show the significant effect of pore plugging and of geometrical exclusion effects on the performance of fixed-bed reactor in the Synthoil process.

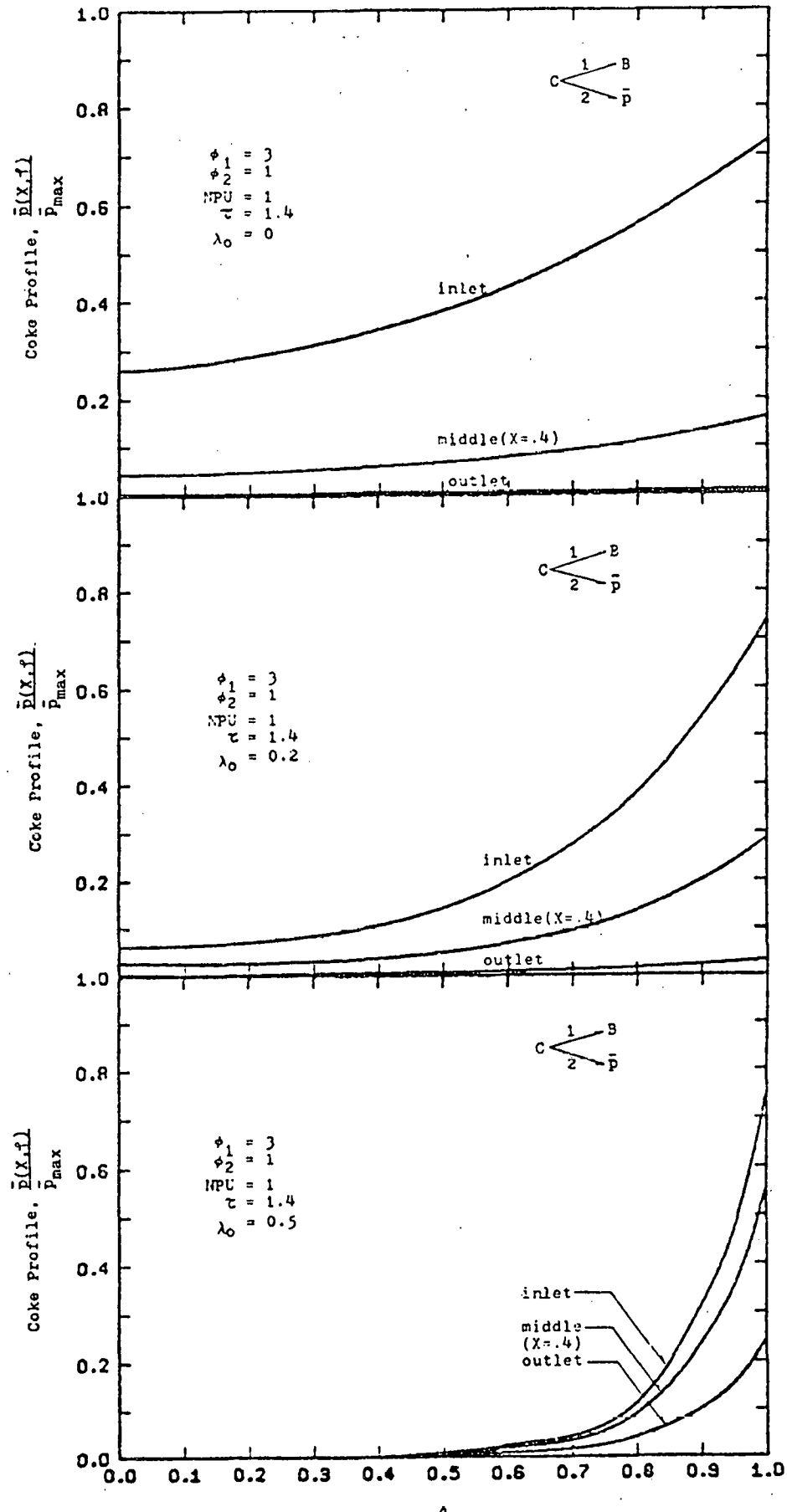

Fig. 18

Comparison of coke profiles inside catalyst pellet at inlet, middle (X = 0.4) and outlet sections of the fixed bed reactor for parallel mechanism.

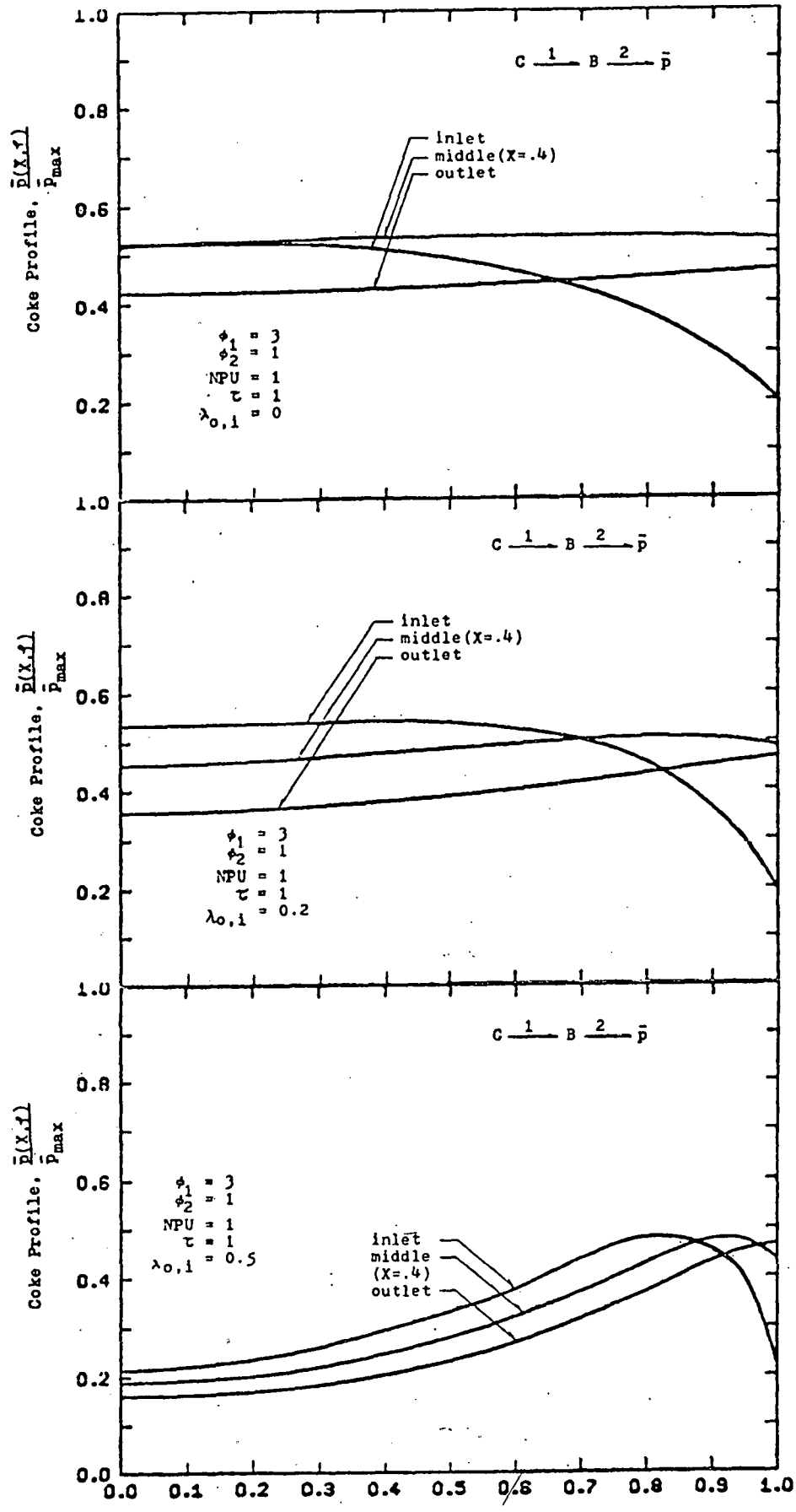

Fig. 19

Comparison of coke profiles inside catalyst pellet at inlet, middle (X = 0.4) and outlet sections of the fixed bed reactor for series mechanism.

Fig. 19

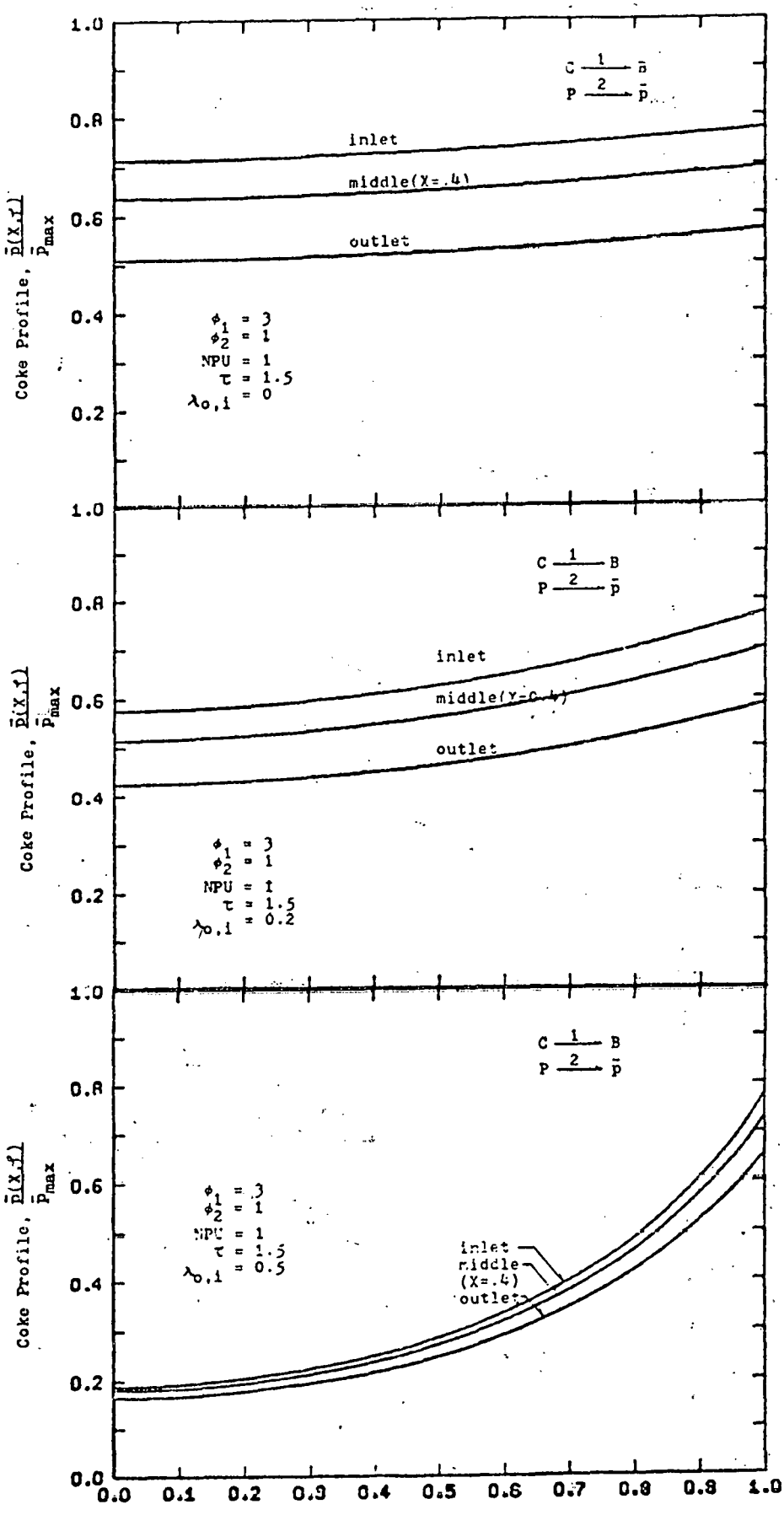

Fig. 20

Comparison of coke profiles inside catalyst pellet at inlet, middle (X = 0.4) and outlet sections of the fixed bed reactor for independent mechanism.

Fig. 20

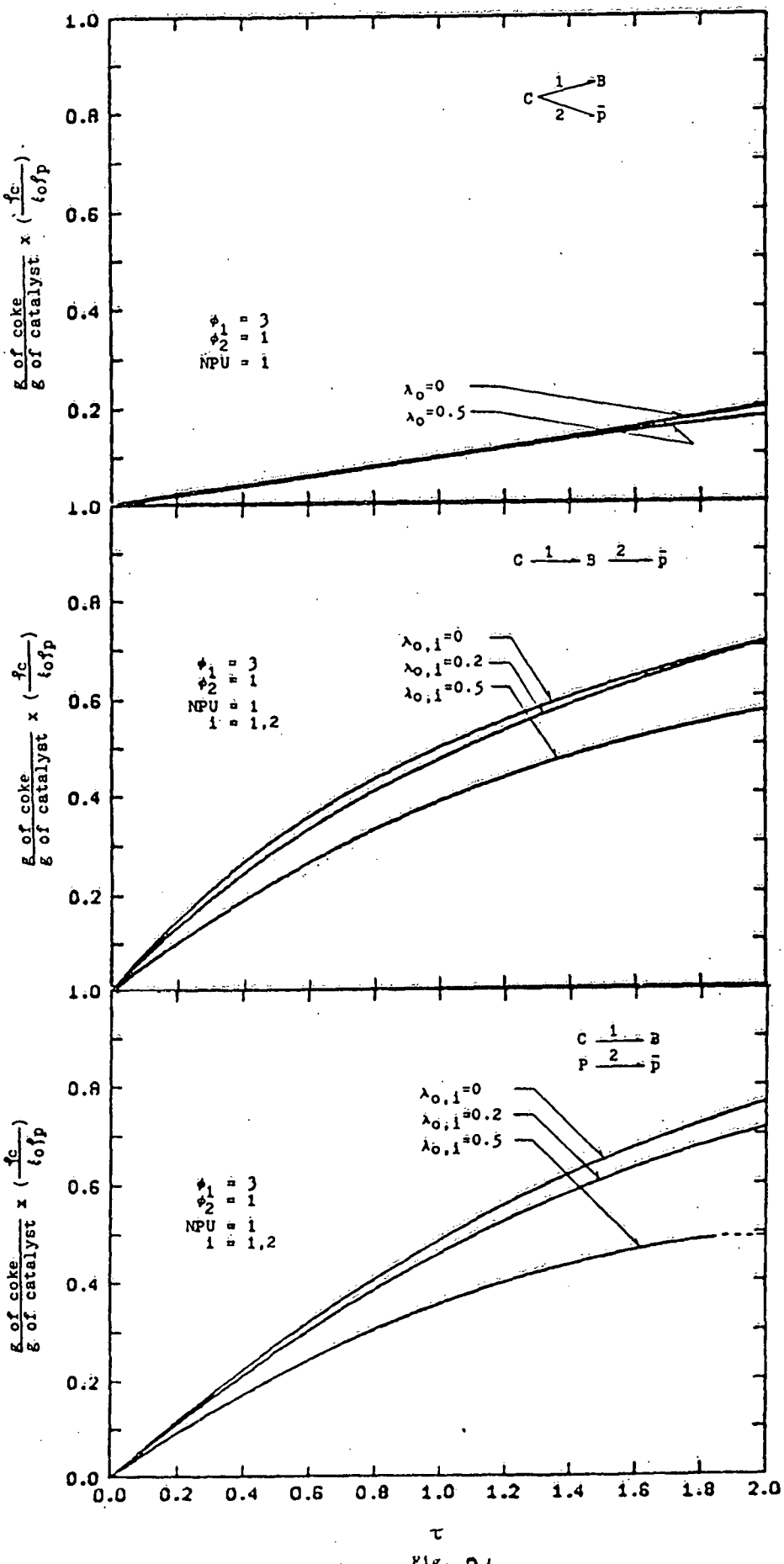

Fig. 21

Propagation of coke accumulation for parallel, series and independent mechanisms respectively.

Fig. 21

These studies of the prototype mechanisms in the Synthoil process combined with that reported previously for the H-coal process will yield the basic characterization for further studies of more complicated systems in the hydroprocessing.

E. Progress in the Synthesis and Characterization of Sulfur-Containing and Nitrogen-Containing Compounds

A) Acridine N-Oxide has been prepared from acridine by oxidation with 3-chloroperoxybenzoic acid

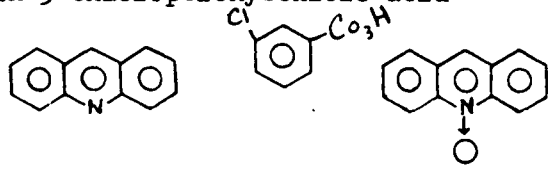

(Markgraf and Ahn, 1964)

B) Benzo[b]naphtho[2,3-d]thiophene has been synthesized by the following sequence of reactions

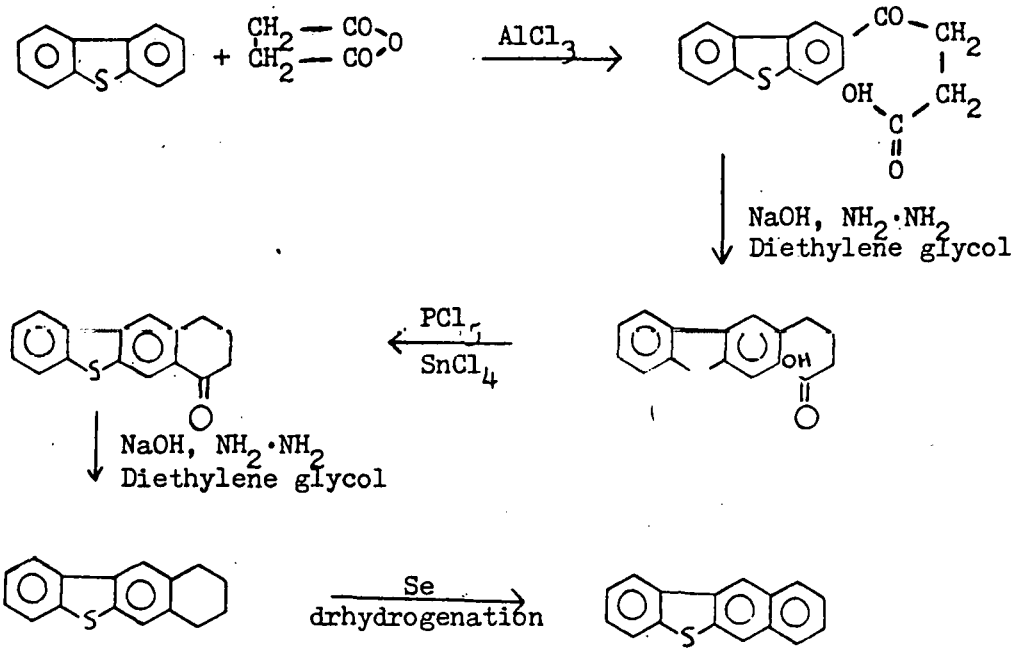

(Campaigne and Osborn, 1968)

C) 7-Methylbenzo[b]naphtho[2,3-d]thiophene has been obtained by the following procedure

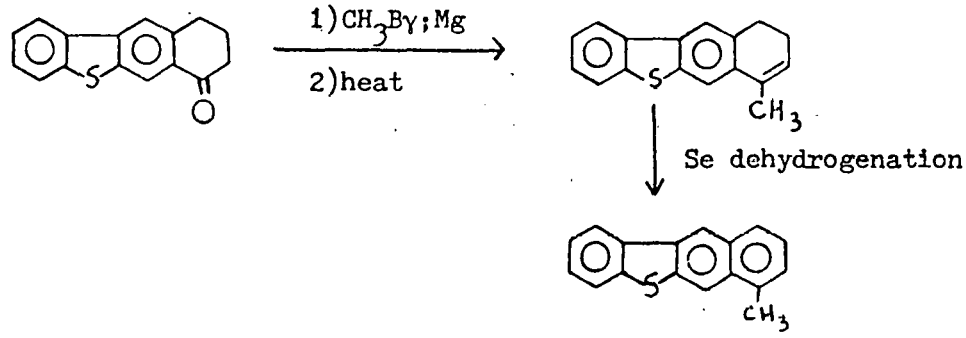

(Campaigne and Osborn, 1969)

D) Thioxanthene has been obtained by the reduction of thioaxanthenone with Lithium aluminum hydride.

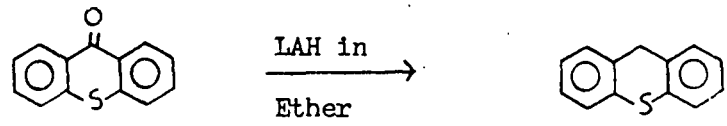

(Mustafa and Hilmy, 1952)

Purification of the product is underway.

Attempt to prepare phenanther[4,5-bcd]thiophene by dehydro-1,4-cycloaddition of sulfur to

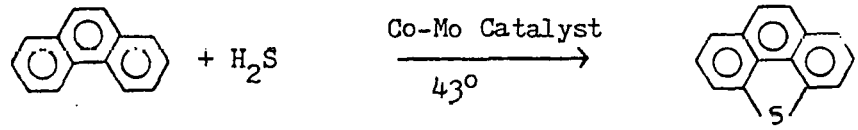

phenanthrene failed.

(Klemn et al., 1970)

An alternative route will be tried as follows

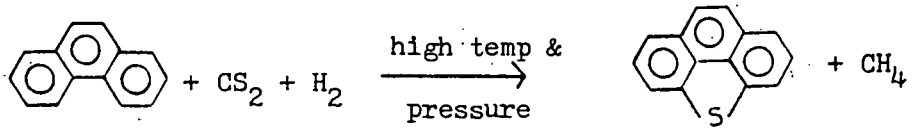

E) 4,6-Dimethyldibenzothiophene has been obtained as follows

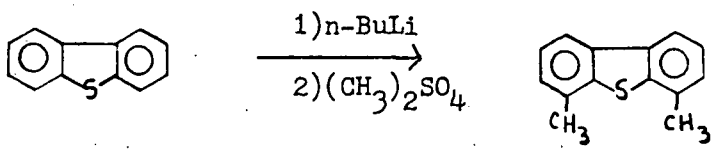

F) Synthesis of 6-Methylbenzo[b]naphtho[2,3-d]thiophene by the following route is in progress.

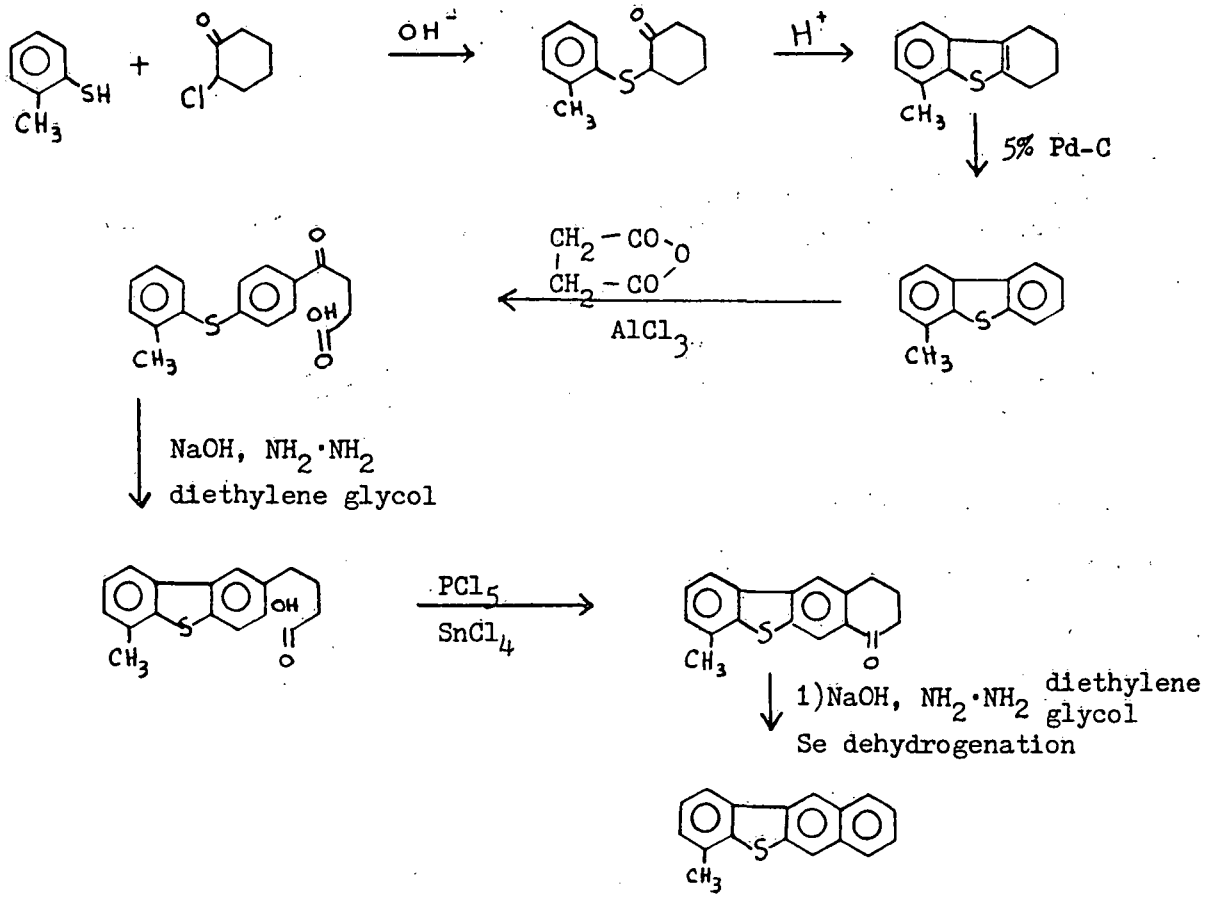

(Campaigne et al., 1969)

G) 4-Methylbenzo[b]naphtho[2,3-d]thiophene will be obtained by methylation reaction

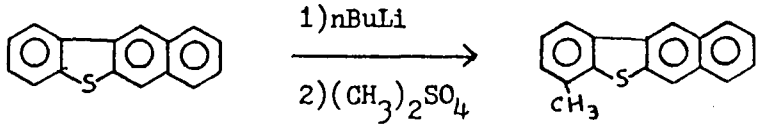

(Litvinov, Gverdtsiteli and Dlubuzh, 1972)

H) Dodecahydrocarbazole will be prepared by progressive reduction of 1,2,3,4-tetrahydrocarbazole.

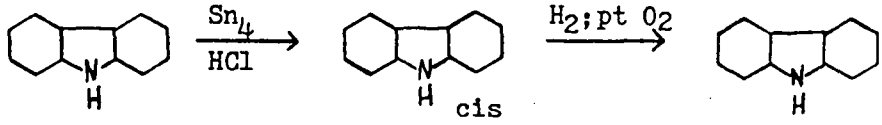

(Gurney, Perkin and Plank, 1927; C. A., 53:5233e)

I) Chromatographic Studies using High-Pressure Liquid Chromatography Techniques

Separation of a mixture of acridine and sym-octahydroacridine has been attempted by high-pressure liquid chromatography using different solvent systems and under varying pressures. We are presently studying ways of effecting separations of the reaction products of hydrodenitrogenation runs, on a scale sufficiently large to secure the isolated products in amounts required for full identification.

NOMENCLATURE

b : Concentration of main product in fluid phase outside the catalyst pellet.

$\tilde{b}$: Concentration of main product in fluid phase inside the catalyst pellet.

$B_{o,i}$: Biot number for ith component, $\frac{K_{f,i} r_c}{D_{e,i}}$.

c : Concentration of reactant in fluid phase outside the catalyst pellet.

$\tilde{c}$: Concentration of reactant in fluid phase inside the catalyst pellet.

c_o : Concentration of reactant at entrance of reactor.

C : Dimensionless concentration of reactant in fluid phase outside the catalyst pellet, c/c_o.

$\tilde{C}$: Dimensionless concentration of reactant in fluid phase inside the catalyst pellet, $\tilde{c}/c_o$.

Cd_i : Correction factor for effective diffusivity for ith component.

dp : Diameter of catalyst particle.

$D_{a,i}$: Axial dispersion coefficient.

$D_{e,i}$: Effectivity diffusivity as defined in equation (7).

K_1 : Rate constant for main reaction.

K_2 : Rate constant for coking reaction.

$K_{f,i}$: Mass transfer coefficient at liquid-solid interface.

L : Length of fixed-bed reactor.

LHSV : Liquid hour space velocity, hr^{-1}.

NPU : Number of poisoning unit as defined in equation (3).

$P_{ec,i}$: Peclet number for ith component (Hdp/Da,i)

p : Concentration of coke precursor in fluid phase outside the catalyst pellet for independent coking mechanism.

$\tilde{p}$: Concentration of coke precursor in fluid phase inside the catalyst pellet for independent coking mechanism.

p_o : Concentration of coke precursor at entrance of reactor.

P : Dimensionless concentration of coke precursor in fluid phase outside the catalyst pellet, p/p_o.

$\tilde{P}$: Dimensionless concentration of coke precursor in fluid phase inside the catalyst pellet, $\tilde{p}/p_o$.

$\bar{p}$: Coke deposition on catalyst surface, g-mole coke/cm^3 of catalyst.

$\bar{p}_s$: Saturated coke deposition on catalyst surface.

$\bar{p}_{max}$: Maximum amount of coke deposition to fill the entire pores of catalyst.

R : Radius of pore in aging catalyst.

R_o : Radius of pore in fresh catalyst.

r_p : Radius of catalyst pellet.

r : Spatial variable of catalyst radius.

t : Time variable.

v : Liquid flow rate.

Greek Symbols

α, β : Exponents of the main reaction expression.

δ, γ : Exponents of the coking reaction expression.

τ : Dimensionless time, $\frac{(t \cdot K_2 \cdot y_o^{\gamma})}{\bar{p}_s}$, where y_o represents c_o for series and parallel mechanisms and p_o for independent coking network.

ξ_b : Porosity in fixed-bed reactor.

ξ_o : Porosity of fresh catalyst particle.

θ : Catalyst activity as defined in equation (1).

ϕ_1 : Thiele modulus for main reaction, $r_c \cdot \sqrt{\frac{K_1 \cdot c_o^{\beta-1}}{D_{e,1}}}$

ϕ_2 : Thiele modulus for coking reaction, $r_c \cdot \sqrt{\frac{K_2 \cdot y_o^{\gamma-1}}{D_{e,2}}}$, where y_o indicates c_o for series and parallel mechanisms and p_o for independent network.

ρ : Dimensionless radius of catalyst particle, r/r_c.

ρ_c : Density of catalyst.

ρ_p : Density of coke deposition.

λ_i : Geometrical ratio of the radius of reactant to the radius of catalyst pore as defined in equation (4).

$\tau_{p,i}$: Time constant for diffusion in catalyst particle for ith component, $\frac{r_c^2}{3 \cdot D_{e,i}}$, hr.

ψ_i : Dimensionless group defined to be $(\frac{1}{pec,i})(\frac{dp}{L})$.

Θ_i : Dimensionless group defined to be $(\frac{1-\epsilon_b}{\epsilon_v})(\frac{Bo,i}{LHSV \cdot \tau_{p,i}})$

Subscripts

s : Concentrations on external catalyst surface.

References

Bartsch, R. and C. Tanielian, "Hydrodesulfurization Hydrogenolysis of Thiophene and Dibenzothiophene over $CoO-MoO_2-Al_2O_3$ Catalyst, J. Catal. 35, 353 (1974).

Campaigne et al., J. Heterocyclic Chem. 6, 553, 885 (1969).

Campaigne, E. and Osborn, S. W., J. of Heterocyclic Chem, 6, 885 (1969).

Campaigne, E. and Osborn, S. W., J. Heterocyclic Chem., 1968, 5, 655.

Chem. Abstr. 53:5233e.

Doyle, G. "Desulfurization via Hydrogen-Donor Reactions," ACS Petrol. Meeting, Chicago, August (1975).

Frye, C. G. and J. F. Mosby, "Kinetics of Hydrodesulfurization," Chem. Eng. Progr. 63(9), 66 (1967).

Gurney, Perkin and Plank, J. C. S., 1927, 2676.

Hoog, H., "Analytic Hydrodesulfurization of Gas Oil," Rec. Trar. Chim. 69, 1289 (19

Houalla, M., N. K. Nag, A. V. Sapre, D. H. Broderick, and B. C. Gates, "Hydrodesulfurization of Dibenzothiophene. Catalyzed by Sulfided $CoO-MoO/\gamma-Al_2O_3$: The Reaction Network, AIChE Journal (1978) communicated.

Klemn, L. H., et al., J. Heterocyclic Chem., 7, 1347, 1970.

Landa, 3. and A. Mrukova, "On the Hydrogenolysis of Sulfur Compounds in the Presence of Molybdenum Sulfide (In German) Col. Czech. Chem. Commun. 31, 2202, 1966).

Litvinov, V. P., Gverdtsiteli, D. D., and Dlubuzh, E., Izv. Akad. Nauk. SSSR, Ser. Khim 1, 70 (1972).

Markgraf and Ahn, JACS, 86, 2699 (1964).

Mustafa, A. and Hilmy, M. K., JCS, 1952, 1343.

Oboleutsev, R. D., and Mashicina, A. V., Dokl. Akad. Nauk, SSSR, 131, 1092 (196

Papadopoulos, R., and Wilson, M. J. G., Chem. Ind., 6, 427 (1965).

Shih, S. S., Katzer, J. R., Kwart, H., and Stiles, A. B., "Quinoline Hydrodenitrogenation: Reaction Network and Kinetics," Preprints ACS Div. Petrol. Chem. 22, 919 (1977).

Wilson, W. A., Voreck, W. E., and Malo, R. V., Ind. Eng. Chem., 49 657 (1957).

VIII. PERSONNEL

There has been only one change in personnel during this quarter. Dr. R. Sivasubramanian has joined in January, 1978, as a post-doctoral fellow.

*U.S. GOVERNMENT PRINTING OFFICE :1979 O-620-097/2225